TAMPEREEN TEKNILLINEN YLIOPISTO
TAMPERE UNIVERSITY OF TECHNOLOGY

ZHIQI YAO

COMPARISON OF STRUCTURES AND PROPERTIES OF ARC-MELTED AND INDUCTION-MELTED HIGH ENTROPY ALLOYS

Master of Science thesis

Examiner: Associate. Prof. PASI PEURA
Dr. Tech. MIKKO HOKKA
Examiner and topic approved by the Faculty Council of the Faculty of Materials Science on 17th August 2016

ABSTRACT

ZHIQI YAO: Comparison of structures and properties of arc-melted and induction-melted high entropy alloys

Tampere University of technology
Master of Science Thesis, 54 pages
August 2016
Master's Degree Programme in Materials Engineering
Major: Material Science
Examiner: Associate Professor Pasi Peura, University Lecturer Mikko Hokka

Keywords: High entropy alloys, casting methods, microstructures, mechanical properties.

High entropy alloys contains five to thirteen different kinds of metallic elements which have different mechanical properties compared to the conventional alloys. Generally, high entropy alloys are manufactured firstly by melting the requested metals by arc-melting or induction-melting and then casting in different atmospheres. It is interesting to know whether the HEAs manufactured in different methods show similar structures and properties.

In this master's thesis, the arc-melted $Al_{0.5}CrFeCoNiCu$ is chosen as the reference sample. Meanwhile, induction-melted $Al_{0.5}CrFeCoNiCuMo_{0.25}$ and $Al_{0.5}CrFeCoNiCu$ which casted in air and vacuum condition are studied also for finding out whether $Al_{0.5}CrFeCoNiCu$ HEAs with desired properties can be manufactured by this way. The microstructures of HEA samples were observed with optical microscope and scanning electron microscope while the crystalline structure was studied by X-ray diffraction. Afterwards, the compression test was carried out to obtain mechanical properties of HEAs.

By SEM, it could be seen that HEA samples had similar composition distribution. However, dark spots which contains sulfur inclusion could be found in induction-melted samples. The induction-melted $Al_{0.5}CrFeCoNiCu$ HEAs had a bcc+fcc structure and showed more brittle. By contrast, the induction-melted $Al_{0.5}CrFeCoNiCuMo_{0.25}$ HEAs had a fcc crystalline structures and showed good ductility. In summary, the induction-melted $Al_{0.5}CrFeCoNiCu$ HEAs samples showed relatively poor mechanical properties compared to reference samples. In order to alter this condition, since the mechanical properties are related to the cooling rate and impurities, it is recommended to control the cooling rate and reduce the amount of impurities.

PREFACE

This study represents a big step towards my following life. I would like to appreciate everyone who provided help to me during this time.

I would like to thank Mr. Pasi Peura who has been extremely professional on guiding me during the whole project. He provided excellent ideas about dealing with the specific problems during the project. Mr. Mikko Hokka also helped me with compression test and X-ray diffraction part. I also want to thank Mr. Madan Patnamsetty who helped me a lot during the experiments. He has a deep understanding about the knowledge we need and he is a skillful operator when doing the sample testings. Also, I want to thank the other staff and students for their patience and help.

The reference samples are provided by Assistant Professor Sheng Guo from Chalmers University of Technology. I would like to thank him for his contribution to this work.

The most important thing I got from this project is that the ability to overcome the diffculties when facing the unknown hinder and alter the plan. It is not a easy thing for me but at least I learnt a lot during this project.

Tampere, 01.11.2016

Zhiqi Yao

LIST OF SYMBOLS AND ABBREVIATIONS

HEAs	High entropy alloys
BCC	Body Centered Cubic
FCC	Face Centered Cubic
S	Entropy
H	Enthalpy
G	Gibbs free energy
R	Gas constant
N_A	Avogadro's number
n	Total number of principle elements
C	Number of components
F	Degree of freedom
P	Number of Phases
SEM	Scanning electron microscopy
DAS	Dendrite arm spacing
XRD	X-ray diffraction
VEC	Valence electron concentration
DSC	Differential scanning calorimetry
EDS	Energy-dispersive X-ray spectroscopy
EHT	Electron high tension
AsB	Angle selective backscatter
e	Engineering strain
ε	True strain
σ_e	Engineering stress
σ_{true}	Engineering stress

Table of Content

1. INTRODUCTION 1
2. STRUCTURE AND PROPERTIES OF HIGH ENTROPY ALLOYS 3
2.1 Core effect 3
2.1.1 High entropy effect 3
2.1.2 Severe lattice distortion effect 5
2.1.3 Sluggish diffusion effect 6
2.1.4 Cocktail effect 7
2.2 Manufacture of HEAs 8
2.2.1 Arc melting 8
2.2.2 Induction melting 9
2.2.3 Soild-state powder processing 10
2.2.4 Magnetron sputtering 11
2.3 Structure of HEAs 12
2.3.1 Crystalline structure of HEAs 12
2.3.2 Microstructure of HEAs 15
2.4 Mechanical properties of HEAs 18
2.5 Other properties 20
2.6 Applications of HEAs 25
3 EXPERIMENTS METHODS 26
3.1 HEA Samples 26
3.2 Testing methods 27
3.2.1 Optical microscopy and scanning electron microscopy 27
3.2.2 X-ray diffraction 28
3.2.3 Hardness testing 29
3.2.4 Compression testing 30
4 RESULTS AND DISCUSSION 32
4.1 Optical microscopy images 32
4.2 SEM images 33
4.3 EDS mapping 37
4.4 X-ray diffraction 41
4.5 Hardness test 44
4.6 Compression tests 46
5 CONCLUSION 53

6 REFERENCES 55

1. INTRODUCTION

Currently, high entropy alloys (HEAs) are interested because of their special structures and high performance in mechanical properties. High entropy alloys are the alloys which consists at least five different principal elements. The atomic percents of each element are in equal or near equal. Normally, high entropy alloys behave higher mechanical properties and also have good corrosion and oxidation resistance compared to conventional alloys. Although the idea of HEAs was published before 2004, the research was accelerated after 2010. Therefore, HEAs are a kind of new material which has flexible composition and adjustment properties. It is also insteresting to see how the properties change by adding the different additional elements into basic metals (aluminum or iron) during manufacturing of HEAs. As the Fig.1.1 shows, as the increasing of n, total number of equiatomic compositions experience a dramatic increasing. When n reached to 16, almost 10^4 of equiatomic compositions can be found. Therefore, it brings a large amount of posibilities to the researchers who study HEAs.

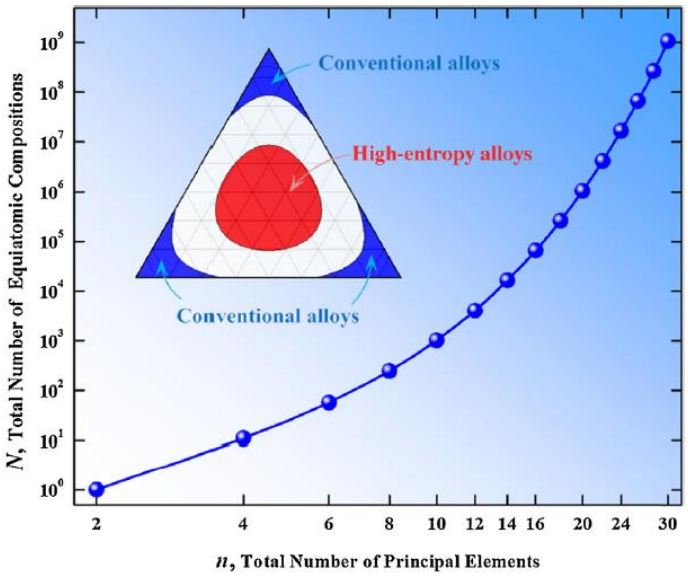

Fig.1.1. *The relationship between total number of equiatomic compositions and total number of principal elements. [1]*

The structures and properties of high entropy alloys are influenced by a large amount of parameters. For instance, casting atomosphere, composition of different elements during

melting and heat treatments after manufacturing all have impacts on structures and properties of high entropy alloys. Generally, high entropy alloys are manufactured by arc-melting or induction-melting casting. The obtained products may have different structures and mechanical properties. Arc-melting has a high vacuum level which is benificial to avoid of impurities while induction-melting is easy to control and can prevent alloying loss to some extend. In this project, the main aim is to compare the structures and mechanical properties of HEAs melted by arc-melting and induction-melting. In this work, different kinds of samples are chosen: arc-melted $Al_{0.5}$CrFeCoNiCu HEA, induction-melted $Al_{0.5}$CrFeCoNiCu HEA and induction-melted $Al_{0.5}$CrFeCoNiCu$Mo_{0.25}$ HEA are studied.

In this study, the microstructures of HEAs are observed and analyzed by optical microscope and scanning eletron microscope while the crystalline structures are determined by X-ray diffraction. After that, hardness and compression tests are applied to find out the mechanical properties of HEAs. By combining the microstructures and mechanical properties, the conclusion can beobtained. It is also interesting to see whether the induction-melted $Al_{0.5}$CrFeCoNiCu HEA shows similar microstructures and properties when compared to arc-melted $Al_{0.5}$CrFeCoNiCu HEA. If not, it is important to see what happened to the final products and what should be done to alter this condition. As for $Al_{0.5}$CrFeCoNiCu$Mo_{0.25}$ HEA samples, it is desired to know whether the addition of molybdenum change the mechanical properties of HEAs.

2. STRUCTURE AND PROPERTIES OF HIGH ENTROPY ALLOYS

This chapter will describe the structures and properties of high entropy alloys. The description is beginning with four core effects of HEAs: high entropy effect, severe lattice distortion effect, sluggish diffusion effect and cocktail effect as well. Then it lays out some basic methods of manufacture of HEAs, among which the arc-melting and induction-melting are the most vital processings to the whole project. Afterwards, both the crystalline structures and microstructures are discussed according to the previous published literature. Next, the mechanical properties of HEAs are also introduced as it is important to find out the specific mechanical property before applications. Genarally, HEAs have higher mechanical properties and corrosion resistance compared to traditional alloys. Finally, some mordern applications about HEAs are figured out.

2.1 Core effect

Compared to conventional alloys, HEAs have four core effect: high entropy effect, severe lattice distortion effect, sluggish diffusion effect and cocktail effect.

2.1.1 High entropy effect

According to Gibb's phase rule, the Gibbs free energy of HEAs can be calculated by the following equations: [2]

$$\Delta G_{mix} = \Delta H_{mix} - T\Delta S_{mix} \qquad (2\text{-}1)$$

$$\Delta S_{mix} = -R\sum_{i=1}^{N} c_i \, lnc_i \qquad (2\text{-}2)$$

$$\Delta H_{mix} = \sum_{i=1, i\neq j}^{N} 4\Delta H_{AB}^{mix} c_i c_j \qquad (2\text{-}3)$$

N is the number of component, R is the ideal gas constant. The c refers to atomic fraction. Alloys that contain several different metallic elements tend to form brittle and complex structures. Gibbs phase rule describes the number of phases (P) in the known alloy at constant pressure in equilibrium system as: [2]

$$P = C + 1 - F \qquad (2\text{-}4)$$

Where C is the number of metallic elements and F is the maximum number of thermodynamic degrees of freedom in the given system. [2] When pose a 5-component system as an example, the possible number of equilibrium phases is six accrodding to the equation. However, high entropy alloys consist of only a few solid solution phases surprisely which is far lower than the maximum value given by Gibbs phase rule. This situation can be explained as the high mixing entropy existed in HEAs enhances the solubility among elements and hinder the possible separation from phase to intermetallic phases. As a result, high entropy alloys tend to form high entropy phases instead of intermetallic phases.

In Fig.2.1, it shows the X-ray diffraction (XRD) patterns of different metallic systems which indicates that the number of phases does not experience an increasing as the number of elements increasing. Only one simple phase can be observed in CuNiAlCoCrFeSi system.

Higher mixing entropy corresponding to higher number of elements of equimolar alloys according to the figure. HEAs have signicicantly high mixing elements than that of conventional alloys which is benificial to form solid solution phases with simple microstructures. Therefore, the number of phases is reduced. Not like the intermetallic compounds, solid solution phases are more ductile.

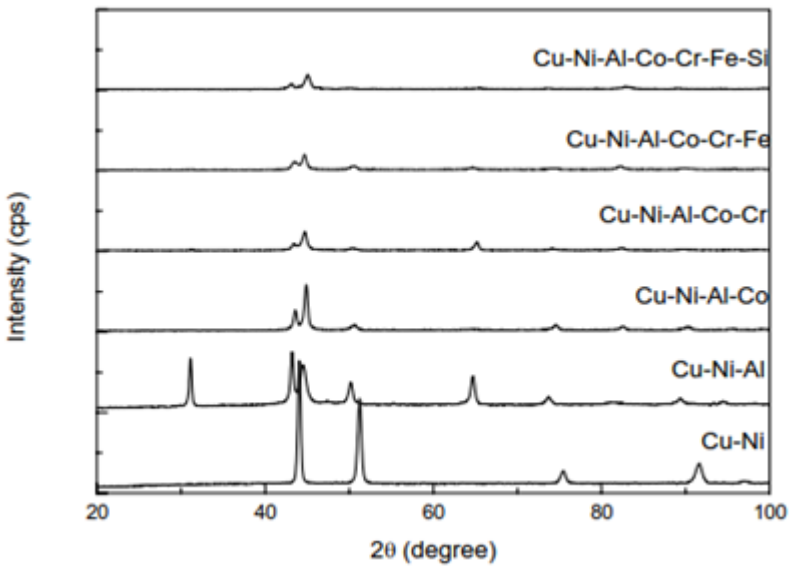

Fig.2.1. *XRD patterns of several element equimolar alloys.[2]*

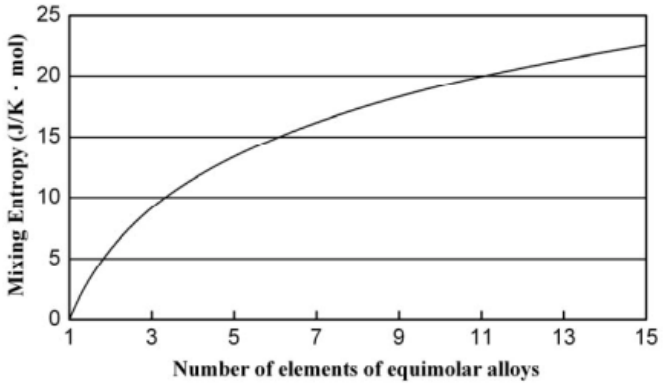

Fig.2.2. *The relationship between number of elements and mixing entropy. [2]*

2.1.2 Severe lattice distortion effect

High entropy alloys consists of several different elements which leads to a multicomponent matrix. The differences in atomic size cause the lattice stress and strain when the atoms are positioned in this kind of matrix. Also the diverse bonding energy and crystalline structures contribute to the severe lattice distrotion. Compared to the conventional metallic matrix, critical lattice distortion can be observed in HEAs matrix. In Fig.2.3, it indicates the severe lattice distrotion of a bcc lattice consists of five elements which is highly distorted compared to a conventional unit cell.

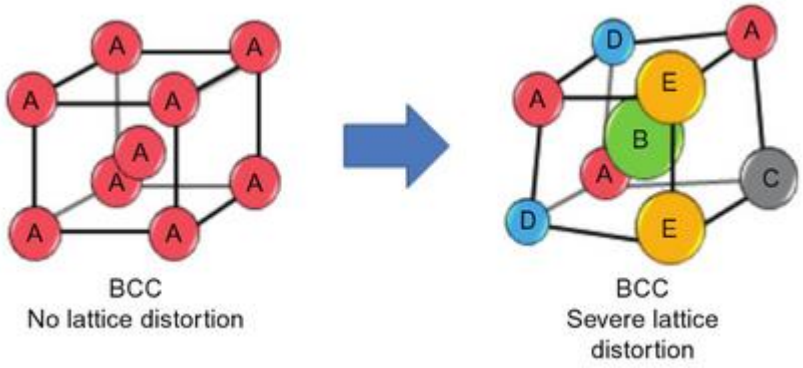

Fig.2.3. *The conventional bcc unit cell contains just one element and severe lattice distortion condition observed in bcc unit cell contains five different elements.*

Lattice distortion strongly affects the mechanical properties of HEAs alloy. The heavily distorted lattice leads to a solution hardening which makes the alloy harder and tougher. The measured Vickers hardness of the HEAs is higher than that of obtained by mixture rule. This condition is more severe in FCC alloys. As the FCC lattice has 12 neighbors while BCC

lattice has only 8 neighbors, FCC lattice suffers from heavier distrotion than that of BCC lattice. [3]

Also the thermal properties are influenced by lattice distrotion. Lattice distortion reduces the thermal conductivity of alloys as a result of the reduction of electron contribution. In summary, severe lattice distortion effect provides higher strength, higher hardness to HEAs. [3]

2.1.3 Sluggish diffusion effect

Sluggish diffusion effect is used to describe the comparison of diffusion paramters between conventional alloys and high entropy alloys. Accroding to the previous researches, HEAs have the lower diffusion rate than that of stainless steels and pure metals. The nuclei of HEAs system is easier to form but grow slowly due to the sluggish diffusion effect, nano-sized precipitations are obtained as a result. [4]

In order to figure out the the differences of diffusion rates between a HEAs system and pure metals, CoCrFeMnNi alloy system with the fcc structure has been studied. [4]

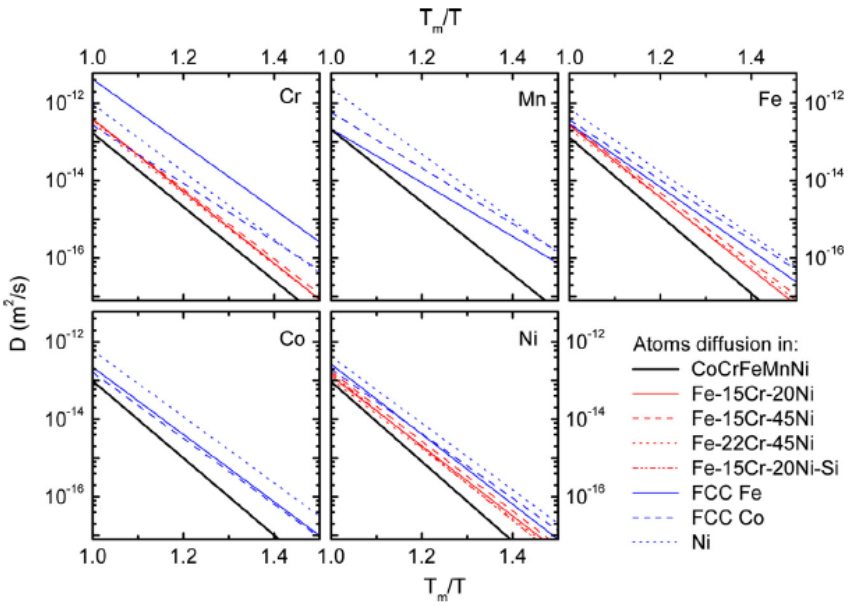

Fig.2.4. *Interdiffusion coefficients D for Co, Cr, Fe, Mn, Ni and Si alloy in different matrices. [4]*

From Fig.2.4, it can be seen that CoCrFeMnNi alloy system has the very low diffusion coefficient compared to other metallic systems. The diffusion coefficient is also correlated with the compositions of different elements. Low diffusion rates make the microstructures of HEAs more complicated. The constitution of HEAs may include ordered solid-solution

phases, disordered solid-solution phases, amorphous phases and also nano-sized precipitates. With SEM and TEM, the size of the final particles can be measured which helps to find out the nano-sized precipitates. The fine precipitation could increase the toughness and strength of HEAs. Also the creep resistance can be improved to achieve a longer life time of alloy products. [4]

2.1.4 Cocktail effect

Cocktail effect can be described as an enhancement of the mechanical properties of HEAs by their constituents. High entropy alloys have ideal hardness and toughness properties compared to the conventional alloys. Moreover, some unexpected properties can also be obtained by mixing different elements, which could not be observed in the individual element.

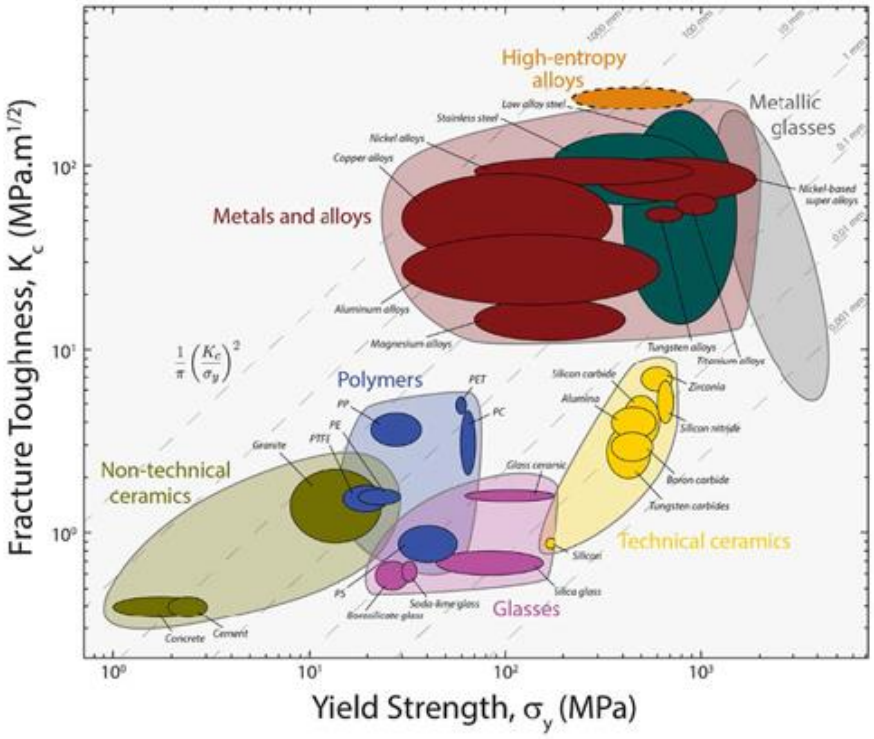

Fig.2.5. *HEAs show an excellent combination of yield strength and fracture toughness as the result of cocktail effect. [5]*

From Fig.2.5, it can be concluded that the HEAs have the high fracture toughnesss and high yield strength among the mentioned materials. In addition to the high strength properties, other enforced parameters such as a wide range of Young' modulus are reported also. Moreover, high electrical resistance and low coercivity can also be brought to HEAs due to cocktail effect. The enhancement of the properties offers a wide range of applications for HEAs. [5]

2.2 Manufacture of HEAs

Most high entropy alloys are manufactured by vacuum arc melting, induction melting.

2.2.1 Arc melting

Vacuum arc melting is the method in which an electric arc is used to melt the metallic materials within the vacuum container.

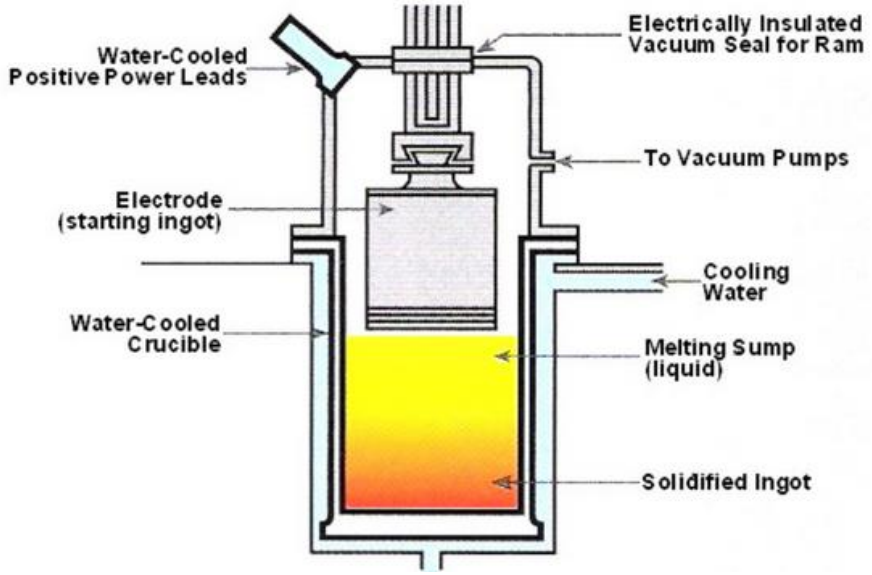

Fig.2.6. *The equipment of vacuum arc melting. [6]*

Fig.2.6 shows the equipment of vacuum arc melting processing. The electric arc contact with the tip of the starting ingot. Then the ingot is melted within a vacuum furnace. As the melted electrode drops into the bottom of that container, the residual gases such as nitrogen and oxygen are removed from the surface of the ingot drops. Thus the properties of the final alloys can be improved significantly. The high ductility and ideal resistance to fatigue can be observed in products when melting in this way. A large amount of steels and metals can be processed by arc melting, such as 9310 steel, Ti-6Al-4V and nickel superalloys. When processing metallic materials in arc melting, it is vital to control the consistency of the melting as the complex thermal transfer may influence the properties of the alloys. [6]

Arc remelting is a processing which is used to refine the structure and minimize the impurities contents of ingot. The continuous remelting of ingot is carried out by arc in a vacuum level. As the products manufactured by induction-melting may have rough structure and defects, arc remelting can be applied to improve the cleanliness. However, the unmelted residues of electrode and the splattering of arc may implant in the ingot which induces the white spots

in the final products. These white spots have significant influence on mechanical properties of HEAs. [6]

2.2.2 Induction melting

Induction melting can be described as the electrically conducting materials melted by electromagnetic induction during which the heat is gathered in the material by Foucault currents. The eddy current melts the bulk materilas by Joule heating.

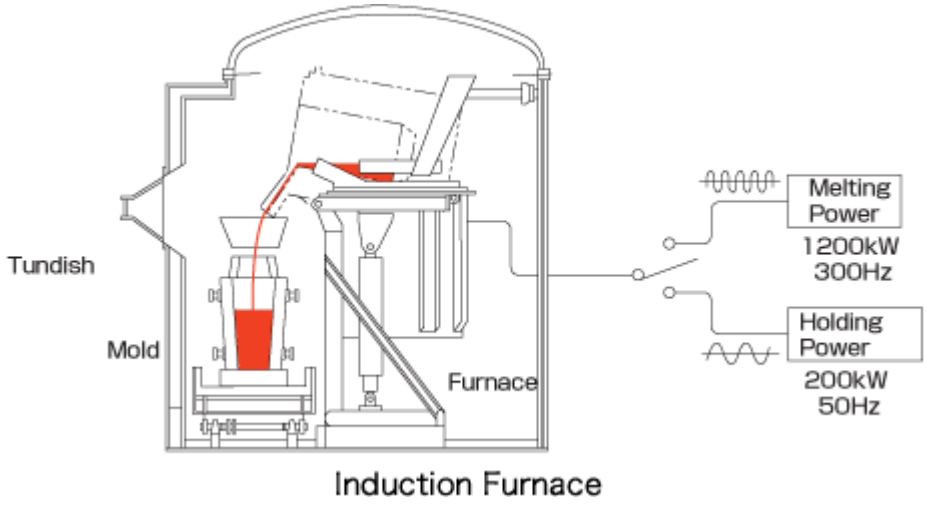

Fig.2.7. *The equipment of induction melting. [7]*

The metallic materials are positioned in the heating furnace where the electromagnetic induction is located in the bottom of the container. As the heat is generated inside the metals, the metals begin to melt rapidly. Then pour the hot liquid to the mold in front of the furnace in a controlled speed. The final products can be obtained after the cooling. It can be used in a inert or vacuum atomosphere. When melting the metals which will oxidize in the air, it is proper to heat them in a vacuum condition. Compared to arc melting, induction melting is easier to control and more energy-efficient. Also alloying loss can be reduced to some extend.[7]

On the one hand, the impurities can be reduced during induction melting by adding the gettering agent such as yttrium and improving level of vacuum. Basically the surface of final products is relatively rough after the vacuum induction melting, heat treatments such as hot rolling can be applied to alter this conditions and refine the grains. On the other hand, induction-melting also has many advantages: the processing parameters like time and temperature are easy to control and also the homogeneity of alloy can be controlled. Also, the alloying losses from oxidation can be prevented to some extend. [7]

2.2.3 Soild-state powder processing

Soild-state powder processing can be used to produce powder particals in a high energy ball mill. Many HEAs are produced by arc melting or casting, however, these methods are not optimal for industrial processing sine the dimension of final metallic productions are restricted. By contrast, mechanical alloying provides a more economic way to fabricate HEAs.

Normally, mechanical alloying involves three seperated stages. The first stage is crushing, metallic elements materials are crushed into fine powders by a ball mill. After that, the fine powder particles are cold welded. The metallic powders are then heated until the sintering occurs and thus the molecular bonds are formed. In this way, HEAs can be obtained without a melting.

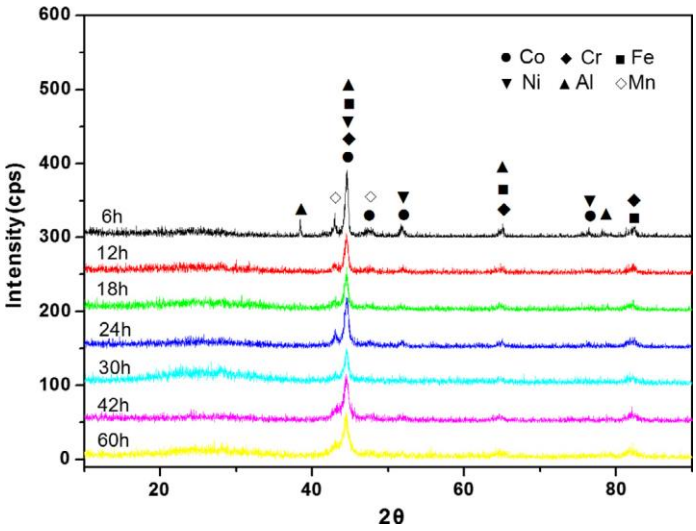

Fig.2.8. *The XRD patterns of mechanical alloyed CoCrFeNiMnAl HEA powder with diverse milling time. [8]*

Figure 2.8 shows an example of XRD results of CoCrFeNiMnAl HEA produced by mechanical alloying methods using a planetary ball mill. During the iniation stage of mechanical alloying, all the diffraction peaks of each metallic element can be observed in XRD patterns. After 6h milling, the intensities of seperated elemental peaks decrease while the intensity of alloy increases. As the milling time increases, some peaks are lossing. This condition indicates that the formation of solid solution. No significant change can be witnessed after 60 h which means the mechanical processing reaches the maximum extent. As a result, the high lattice strain leads to the broading of peaks while the lattice distortion induce the disappearance of initial existed peaks. [8]

2.2.4 Magnetron sputtering

High entropy alloy thin film can be deposited from an alloy target or a mosaic target. Magnetron sputtering is a method which can reduce the compositional error in high numbers of metallic elements alloys. It provides a way for ejected atoms from metallic materials to be cooled in high vacuum and condense on substance thus form a thin film upon the material. Thus, a tightly bound atomic layer can be formed. In order to enhance the sputtering processing, a magnetron is used to produce a magnetic field around targeted area.

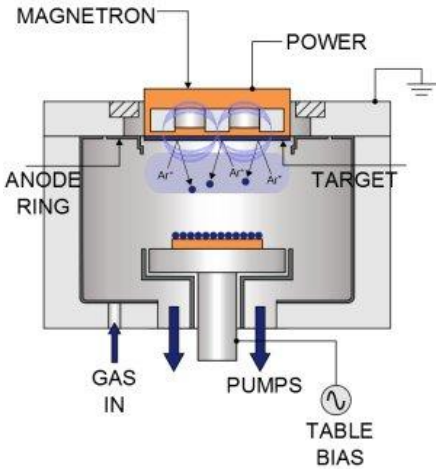

Fig.2.9. *The principle of magnetron sputtering deposition*

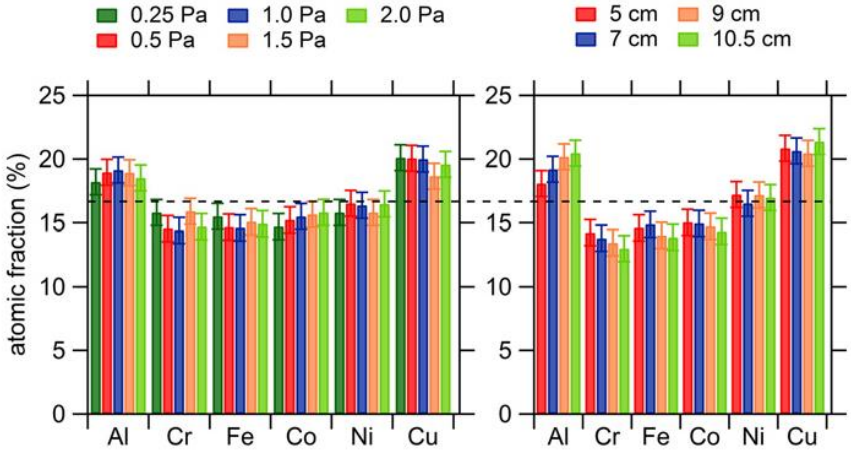

Fig.2.10. *The composition of AlCoCrCuFeNi HEA film deposited at different pressures (left figure) and at different substrate-target distances (right figure)[9]*

AlCoCrCuFeNi HEA films have been produced with different pressure conditions and diverse substrate-target distances. The final atomic fraction of each elements are different according to Fig.2.10. It can be concluded that the sputtering pressure and substrate-target distance are influtial parameters to final compostions of thin film. In this way, compositions

of HEAs can be controlled by altering the deposition pressure and substrate-target distances. [9]

2.3 Structure of HEAs

2.3.1 Crystalline structure of HEAs

HEAs normally consist of minimum five different metallic elements in equal or almost equal atomic percent (at.%). Most HEAs have the crystalline structures as body-centered cubic (bcc) or face-centered cubic (fcc) structure. Although HEAs with a hexagonal close-packed (hcp) structure are seldom reported, it is also possible to observe hcp structure in HEAs. Figure 4.1 gives the example for a hexagonal close-packed structure found in YGdTbDyLu and GdTbDyTmLu alloys. [10]

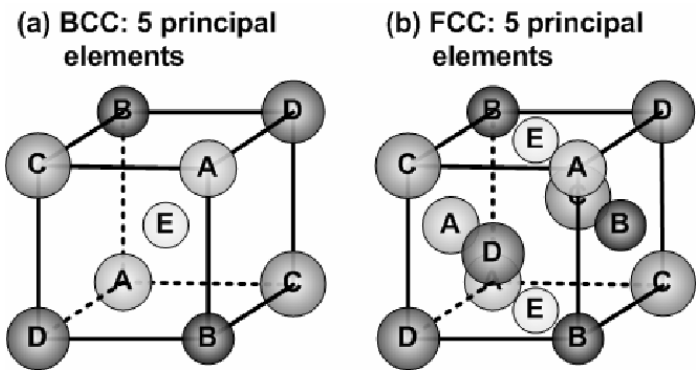

Fig. 2.11. *Basic BCC-structured and FCC-structured solid solution with 5 principle elements. [11]*

As the Fig.2.11 presents, the atoms of different elements arranged in a unit cube with a bcc- or fcc-structure. It is also been said that the dominant parameter for controlling the microstructure in HEAs is the elemental interactions. [12] Two significant parameters conrtributes to estimate the types of cystalline structures: Ni equivalent (Ni_{eq}) and Cr equivalent (Cr_{eq}). The elements like Ni, Mn, N and Cu are bcc stabilizer whereas Cr, Si, Mo are fcc stabilizer according to alloying effects in stainless steels. With the following equation, both Ni_{eq} and Cr_{eq} can be calculated [12]:

$$Ni_{eq} = Ni\% + 0.5Mn\% + 0.25Cu\% \quad (2\text{-}1)$$

$$Cr_{eq} = Cr\% + Fe\% \quad (2\text{-}2)$$

Where the Ni%, Mn%, Cu%, Cr% and Fe% refers to the atomic percent of each element. In HEAs, the higher the Ni_{eq}, the higher the possibility to get a fcc structure. By contrast, higher Cr_{eq} value indicates the tendency to obtain a bcc structure.

Moreover, the valence electron concentration (VEC) also contributes to the estimation of the crystalline structures of HEAs. Valence electron is an electron that preticipates the formation of a chemical bond and it is associated with atoms. VEC describes the number of all valence electrons per number of atoms in the alloy. VEC influence the structures and properties of HEAs. VEC can be obtained by the following equation [13]:

$$VEC = \sum C_i(VEC_i) \qquad (2\text{-}3)$$

Where (VEC_i) is the VEC for the individual element. With the VEC value, phase stability for bcc and fcc can be predicted in HEAs. For HEAs with the VEC value which is higher than 8.0, only fcc phase exists. Conversely, bcc phase becomes the dominant phase once the VEC is lower than 6.8. When the VEC is in a interval between 6.87 and 8.0, a mix phase of bcc- and fcc-structured can be observed.

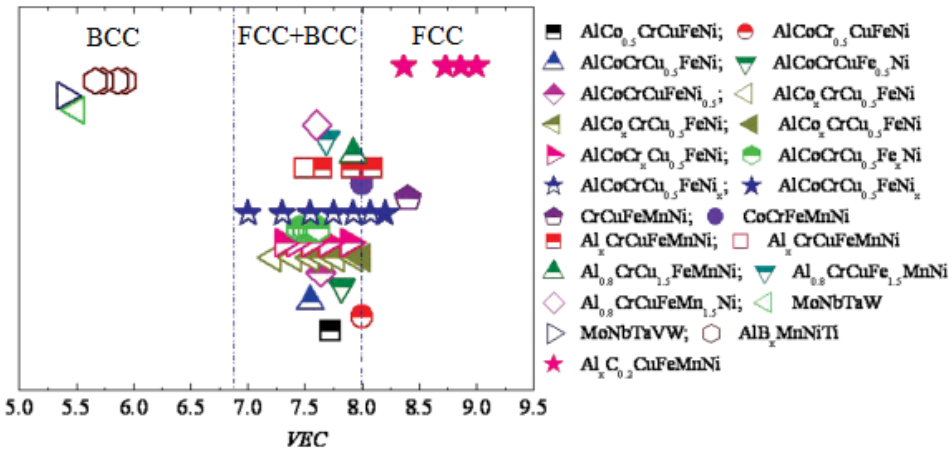

Fig.2.12. *The relationship between VEC and phase stability for HEAs. (The symbols with an empty center refer to bcc phases whereas symbols with fully filled center stand for fcc phases. The intermediate symbols are representation of a mixed phase of bcc and fcc.)[13]*

The Fig.2.12 gives examples of the relationship between VEC and phase stability for HEAs which also provides evidence for the former explanations. Also, sole fcc phase can be found at the boundary. (VEC = 8.0) Therefore, the phase boundaries can be clearly defined by VEC value in spite of some exceptions [13].

The crystalline strucutures can be characterised by X-ray diffraction (XRD). The characteristic peaks in XRD pattern indicates different phases in HEAs.

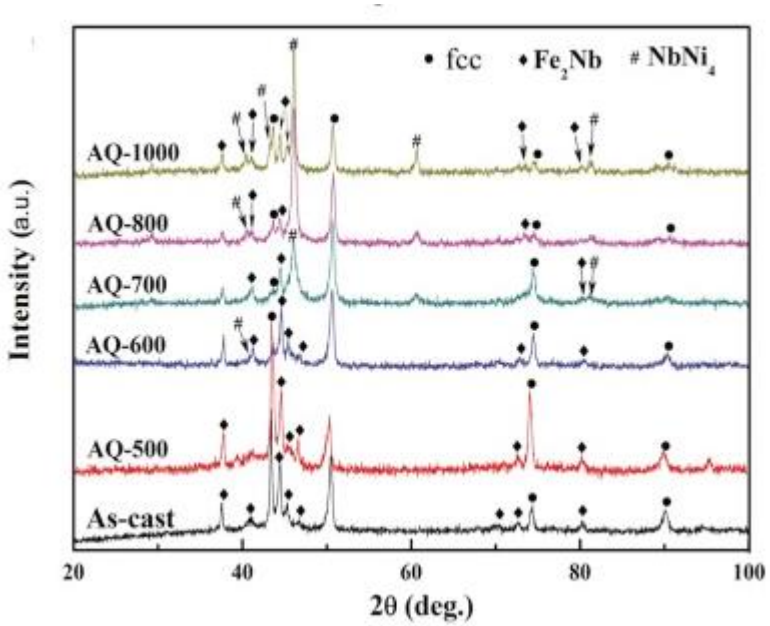

Fig.2.13. *XRD patterns of the as-cast and heat-treated $CoFeNi_2V_{0.5}Nb_{0.75}$ EHEAs.[14]*

Figure 2.13 shows the XRD pattern of the eutectic high entropy alloy named $CoFeNi_2V_{0.5}Nb_{0.75}$. The curves refer to the as-cast and quenched EHEAs (Eutectic HEAs). The Bragg peaks of the bulk and quenched samples can be indexed to be fcc-structured solid solution phase and also Fe_2Nb-type Laves phase. [14]

The content of some specific elements influences the crystalline structures of HEAs. For instance, the content of aluminium is a dominant role in controlling the structures of $Al_xCoCrFeMo_{0.5}Ni$.

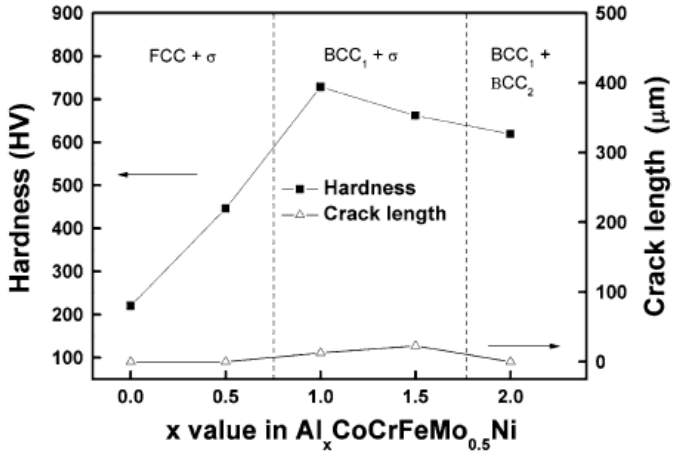

Fig.2.14. *Hardness and total crack length of AlxCoCrFeMo0.5Ni alloys as a function of Al content. [15]*

When the atomic content value of aluminium is lower than 0.75, the phases are tend to be fcc phases and σ phases. As the atomic content value lies between 0.75 and 1.75, it is more easier to get bcc_1 phases and σ phases. The σ phase disappears when the value is higher than 1.75. The bcc_2 phases replaces σ phases to be the new composition.

Normally, the cooling rate may have an effect on the final crystalline structures of alloys. The higher cooling rate leads to smaller grain size and simple structures. [16]

2.3.2 Microstructure of HEAs

The microstructure of HEAs can be analysed with scanning electron microscopy (SEM). With SEM images, the microstructures of HEAs surface and elemental distribution and be examined.

Normally, the surface of HEA contains dendritic (DR) and interdendritic (ID) regions. Precipitates with plate shapes or spherical shapes and nanostructured phases are often found in DR regions. Also, in casted HEAs, elements like copper and aluminum are tend to segregate in ID regions.

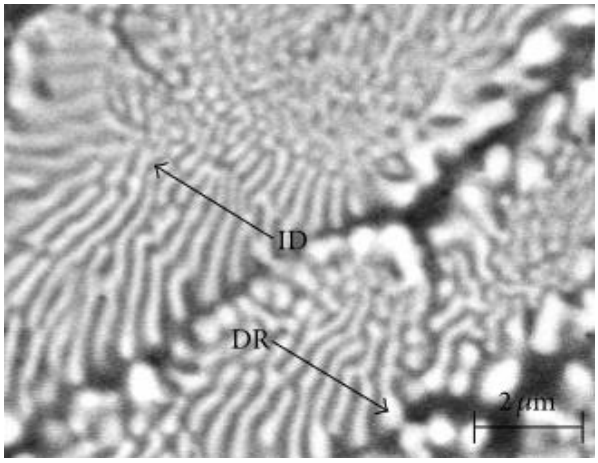

Fig.2.16. *Microstructures of CoCrFeMnNbNi HEA surface which consists dendritic and interdendritic regions. [17]*

Figure 2.16 shows an SEM image of the microstructures of CoCrFeMnNbNi HEA. A lamellar colony formed by dendritic and interdendritic regions can be seen in the image. The dendritic regions show bright in BSI contrast whilst interdendritic regions behave dark as the

arrows signed. The reason for this condition is that DR and ID regions contains different distribution of metallic elements. For DR region, it contains lighter elements like Nb. By contrast, heavier elements like Fe, Cr are distributed in ID regions which results in a dark contrast. [17]

The microstructures of HEAs can be affected by manufacturing condition. Figure 2.17 gives an example of the microstructures of $Al_{0.5}CrFeNiCo_{0.3}C_{0.2}$ HEA powders milled by mechanical alloying with different durations. The initial granular size is smaller than 40 μm according to Fig. 2.17 (a). After 15 h milling, smaller particles form by crushing down the agglomerations. The average particle size reaches at around 10 μm when milling materials for 27 h, then cold weld again the particles after 38 h milling. The crystalline size is reduced while alloying is carried out during this period. Fig. 2.17 (f) shows the final powder after 4 h wet milling in an alcohol milling media. The particle size I much smaller than previous one. The crystalline structures are refined during mechanical alloying.

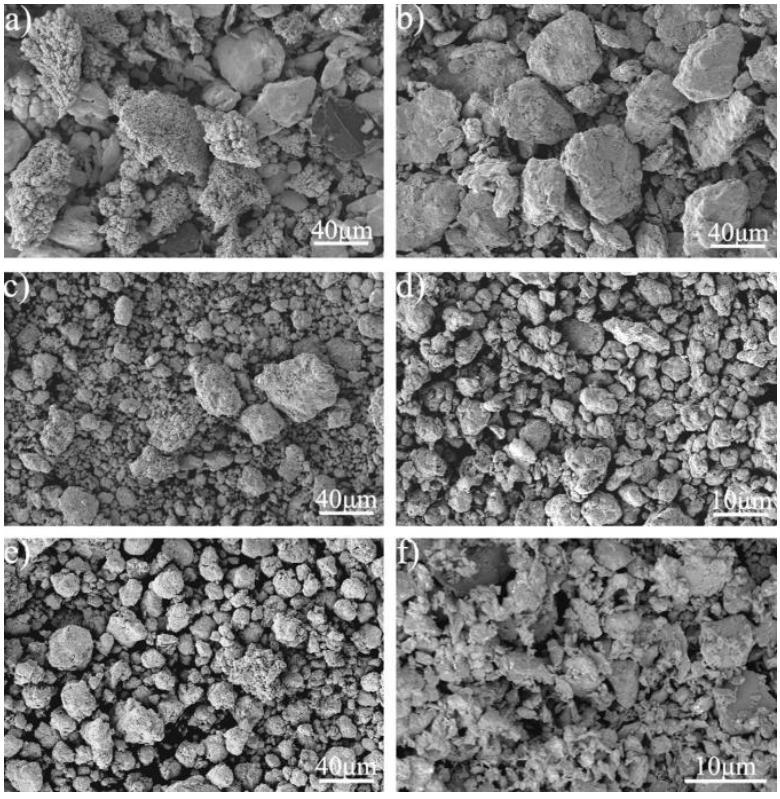

Fig.2.17. *Microstructures of $Al_{0.5}CrFeNiCo_{0.3}C_{0.2}$ HEA powders milled in different time. (a) 0 h, (b) 6 h, (c) 15 h, (d) 27 h, (e) 38 h, (f) 38 h with 4 h wet milled. [18]*

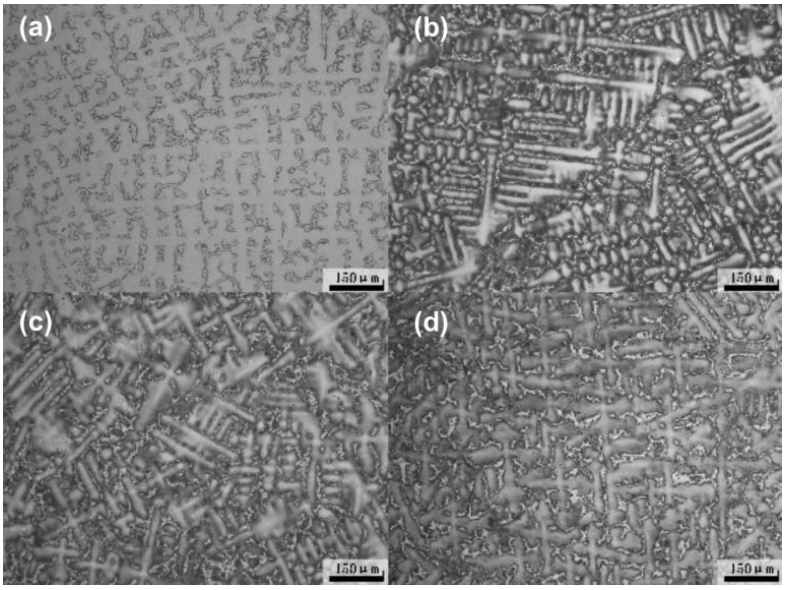

Fig.2.18. *Microstructures of as-casted CoCrFeNiTi0.5 HEA and annealed for 6 h at different temperatures: (a) as-cast, (b) 600 °C, (c) 700 °C, (d) 800 °C. [19]*

Figure 2.18 exhibits the microstructures of as-casted CoCrFeNiTi0.5 HEA with different annealing temperatures. Fig 2.18 (a) shows the surface microstructures of as-cast HEA. In BSI contrast, a large area with bright contrast which is corresponding to dendritic regions can be seen. The arm spacing of dendrite is around 80-150 μm. By contrast, the dark region reffers to interdendritic region which just occupy small amount of areas in the initial stage. After annealing in 600 °C and 700 °C, the significant changes can be observed in images as the ID regions expands whilst the DR region shrinks. The changes are attributes to the released distorted energy and uniformly diffusion form DR region to ID region. Solid solution phases are replaced by intermetallic phases after annealing. [19]

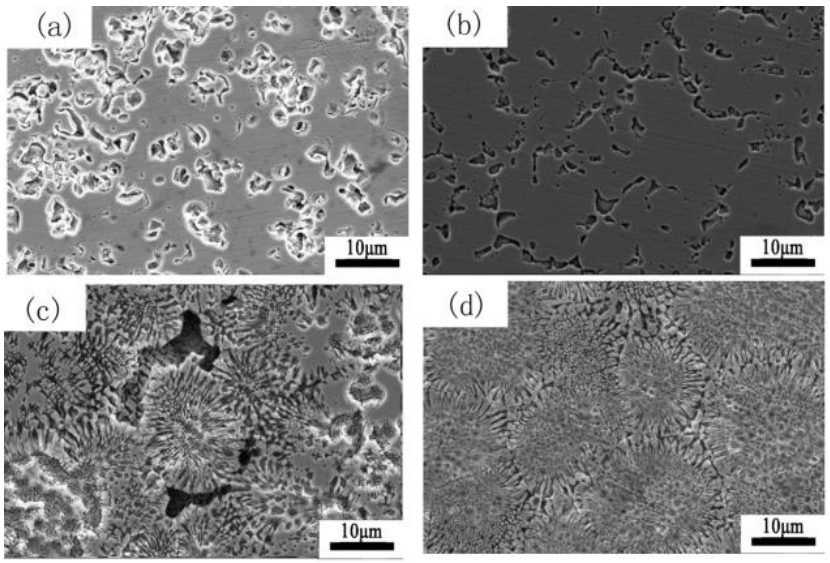

Fig.2.19. *Microstructures of $Al_xCrFeNiTi_{0.25}$ HEAs. (a) Al0, (b) Al0.25, (c) Al0.5, (d) Al0.75. [20]*

The content of aluminum also affect the final microstructures of HEAs. Like typical cast HEAs, DR and IR regions can be found in $Al_xCrFeNiTi_{0.25}$ alloy system. As the content of aluminum raised, more dendrites are formed as a result. Aluminum and nickel mainly segregated into dendritic regions while iron and chromium are uniformly distributed in interdendrite regions. The equilibrium phases are dependent on aluminum content which induce the growth of dendrites. [20]

2.4 Mechanical properties of HEAs

HEAs have high hardness, remarkable wear and corrosion resistance both at room and elevated temperatures. Also, HEAs show high compressive strength and tensile properties.

Several parameters influence the mechanical properties of HEAs. For different HEAs with dissimilar structures, the strength properties are not the same. As for fcc-structured HEAs, the strength is relatively low but plasticity is high. On the other side, bcc-strucured HEAs behave higher strength properties but lower plasticity when compared to the former one. It can be concluded that the crystalline structure of HEAs affects the strength properties. [21]

Not only the intrinsic structure but also the heat treatment method plays a vital role in altering mechanical properties of HEAs. It has been studied that the annealing proceesing influence the hardness of as-cast $AlCrFeNiMo_{0.2}$ HEAs. [21]

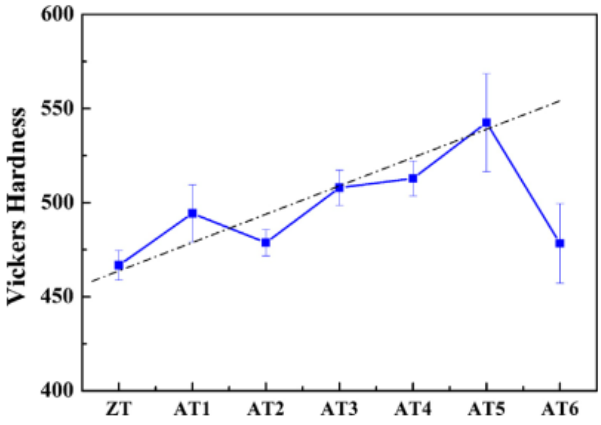

Fig.2.20. *Vickers hardness of as-annealed and as-cast HEAs. [21]*

The curve in Fig.2.20 shows the hardness value after annealing the HEAs at the temperature form 550 ºC to 1050 ºC. (AT1 refers to 550 ºC and AT2 refers to 650 ºC)The inhomogeneous structure induces a slight decrease of hardness at 650 ºC (AT2) . Normally, the hardness

increase gradually from AT2 to AT5(950 ^{o}C). This is because the transfomation from bcc phase to σ phase. The σ phase is an intermetallic compound (Fe-Cr-Ni compound) consists of 30 wt.% Cr~50 wt.% Cr which behaves hard and brittle. The σ phase shows a tetragonal structure and the precipitaion temperature is between 600 ^{o}C and 950 ^{o}C which hcan be used to explain the increasing tendency of hardness during this temperature range. The hardness decreases dramatically after reaching the peak at around 950 ^{o}C (AT5) which can be explained as the disppearance of the σ phase.

Another dominant parameter for cotrolling the strength properties of HEAs is the temperature. At room temperature, the strength is mainly influenced by the crystal structure of HEAs. FCC-structured HEAs have a lower yield strength than that of BCC-structured HEAs. Also, the relationship between cooling rates and strength properties of HEAs has been studied which reported that the final products have a more uniform microstructure and a high ductility after cooling at high rates. Moreover, the different compositions of alloys lead to different mechanical properties.

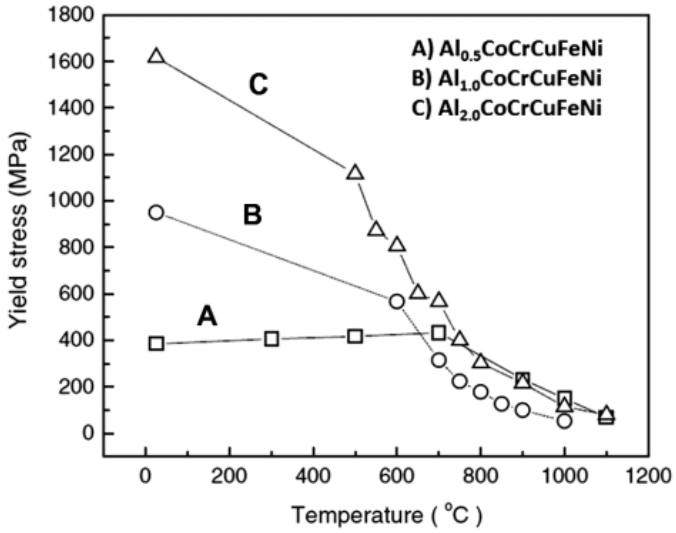

Fig.2.21. *Comparision of yield strength of HEAs determined at diverse temperatures: (A) $Al_{0.5}$CoCrCuFeNi, (B) $Al_{1.0}$CoCrCuFeNi, and (C) $Al_{2.0}$CoCrCuFeNi alloys [21]*

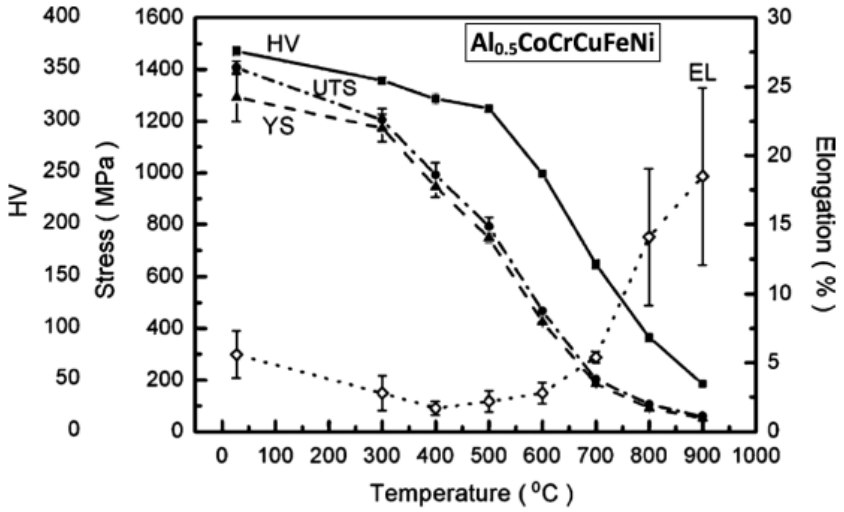

Fig.2.22. *Comparision of hardness, yield strength and elongation of HEAs at different temperatures. [21]*

The mechanical properties of HEAs changed regularly when testing the HEAs at elevated temperatures according to the research results of Yeh. The results are illustrated in Fig.2.22. For Al_xCoCrCuFeNi alloy system, the yield strengh experienced a sharp decreasing along with the increasing of testing temperature. For example, $Al_{2.0}$CoCrCuFeNi alloy has a yield strength as high as 1600MPa at 0°C. However, as the temperature goes up, the yield strength decreases gradually and finally reaches 100MPa at 1100°C. By contrast, the yield strength of $Al_{0.5}$CoCrCuFeNi first experiences a slight increasing as the temperature rising. It reaches the peak at 700 °C and then goes down. The changes of hardness and elongation can also be concluded by figure. The hardness decreases slightly at the initial stage and drops significantly at 500 °C. the elongation also suffers from a slowly decreasing under 400 °C along with the rising temperature. However, the reverse tendency happens after 400 °C. HEAs becomes more ductile and has a higher elongation than that of a bulk alloy. [21]

2.5 Other properties

HEAs can be applied in an amount of industrial applications due to their ideal mechanical properties. Fatigue property, as an influential factor, also affect the lifetime the alloys. The fatigue properties of $Al_{0.5}$CoCrCuFeNi HEA have been studied. [22]

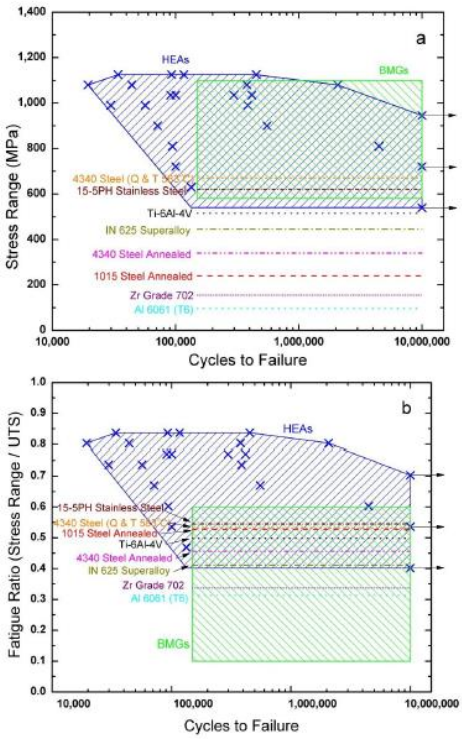

Fig.2.23. *S-N curves of $Al_{0.5}$CoCrCuFeNi HEA and other metallic materials. [22]*

In Fig.2.23, the relationship between faliure cycles and stress range / fatigue ratio of HEAs and other conventional alloys is revealed. In certain cycle before failure, HEAs endure more tensile stress before failure and also have higher fatigue ratio than that of bulk metallic glasses and widely-used steels. The good performance of HEAs can be attributed to their high tensile strength and simple microstructures. The defects can hardly be observed in the internal structures in HEAs as a result of its high mixing entropy. In summary, HEAs can endure more stress and have excellent fatigue resistance when compared to conventional alloys. This provides a chance for HEAs to be applied in aerospace applications due to its longer lifetime and resistance to fatigue.

Wear resistance is a significant parameter in tribological properties of HEAs especially in the conditions where HEAs come into contact with other rough-surface materials. The improved wear resistance has been found in $Co_{1.5}CrFeNi_{1.5}Ti$ and $Al_{0.2}Co_{1.5}CrFeNi_{1.5}Ti$ HEAs. Also, the wear resistance can be enhanced by formation of a smooth wear surface and debris of high hardness. The adhesion wear properties of Al_xCoCrCuFeNi HEAs have been studied. The worn surface is smooth and lay out more fine debris when the content of aluminum is high, which improves the wear resistance as a result. The high hardness of the HEA surface helps to resist the plastic deformation and also contributes to the formation of oxide film. Moreover, the wear behavior of the refractory $Mo_{20}Ta_{20}W_{20}Nb_{20}V_{20}$ HEA has

been studied by sliding the alumina and steel balls on Inconel 718 and $Mo_{20}Ta_{20}W_{20}Nb_{20}V_{20}$ surface respectively. The figure 2.25 shows the results. [23]

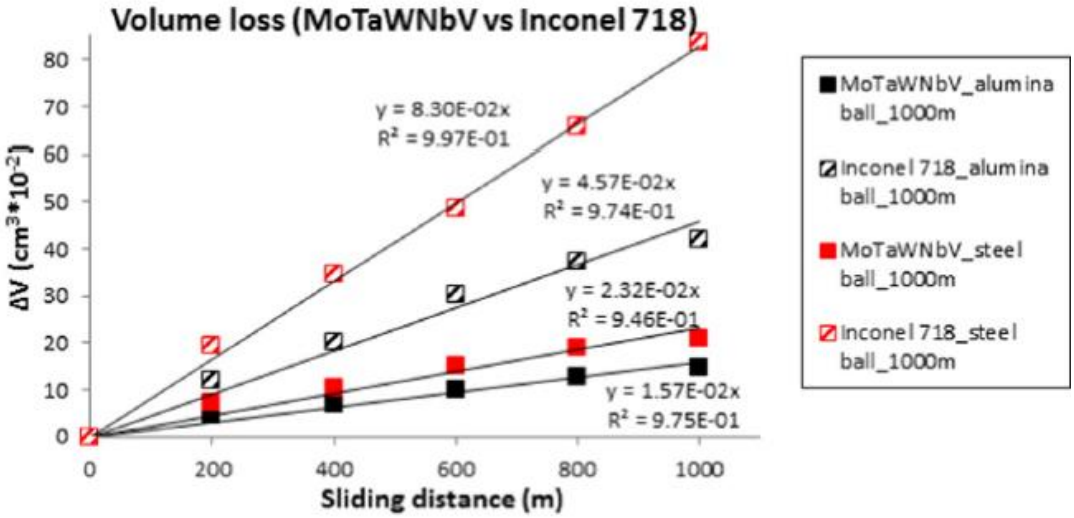

Fig.2.25. *Comparison of the volume loss as a function of the sliding distance and the wear rates for $Mo_{20}Ta_{20}W_{20}Nb_{20}V_{20}$ and Inconel 718. [23]*

$Mo_{20}Ta_{20}W_{20}Nb_{20}V_{20}$ have been reported to have better wear resistance than that of Inconel 718 both with an alumina ball and a steel ball. The volume loss of $Mo_{20}Ta_{20}W_{20}Nb_{20}V_{20}$ is lower than 20% after a long sliding distance (1000m). Thus, it can be concluded that HEAs have better wear resistance than that of some conventional alloys.

Due to high number of alloying elements exist, it is hard to define the melting temperature from literatures. Hence, thermal analysis are carried out to define the melting temperature and thermal expansion coefficient of HEAs. With defined melting temperature, it is easier to select heat treatment methods for HEAs which help to refine the structures and alter the mechanical properties . Usually, the melting temperature of HEAs can be determined by DSC or DTA.

DSC, differential scanning calorimetry, is a widely used method to figure out the thermodynamic properties of materials. DSC can be applied in organic and inorganic samples. In this method, two items named sample and reference are positioned in the same condition as the temperature rising up throughout the procedure. In order to get the reliable results, the reference should equip with a well-defined heat capacity in the scanned temperature range while the temperature of sample holder response linearly to the heating time.

Normally, there are two main types of DSC: Power compensated DSC which has the constant power supply and Heatflux DSC which has the constant heat flux. The results of DSC can be plotted in a DSC curve which reveals the relationship between heat flux and temperature. With DSC curve, the parameters such as glass transition temperature of polymers, melting

temperature can be obtained. For HEAs, the melting temperature can be determined by the endothermic peaks of cooling curve and heating curve. Also, the exothermic peak indicated the solidification of HEAs during the temperature changes. With DSC, the melting temperature and solidification temperature of different phases can be obtained. In this case, DSC can be a sufficient method to limit a temperature range for heat treatments. [24]

Figure 2.26 shows the cooling and heating curves of $Al_{0.5}CrFeCoNiCu$. In heating curve, two obvious endothermic peaks can be seen at around 1150 ºC and 1350 ºC respectively. Two endothermic peaks refer to the melting processing of interdendritic region and dendritic region of HEAs. As for the cooling curve, two main exothermic peaks occur at ~1325 ºC and ~1125 ºC. The peak located in 1325 ºC corresponds to the solidification of dendritic material while the smaller peak in 1125 ºC indicates the formation of interdendrites. [24]

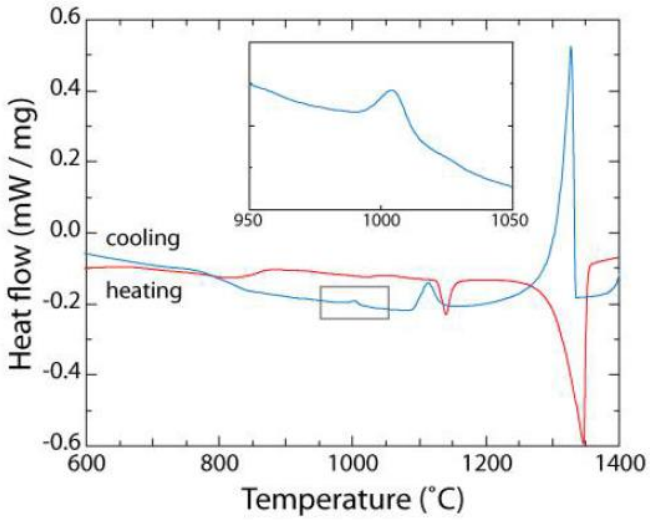

Fig 2.26. *DSC curves of as cast $Al_{0.5}CrFeCoNiCu$ during heating and cooling ($10^oC\ min^{-1}$) [24]*

Also, the thermal properties of HEAs can be detected by DTA (Differential thermal analysis). In DTA anaylsis, the studied material and a reference experience same thermal cycles as the apparatus records the temperature difference betwwen studied material and reference. With DTA, the data such as melting temperature, glass transition and phase transformation can be determined by DTA curves. Not like in DSC, the heat flow for studied material and reference are constant throughout the experiment.

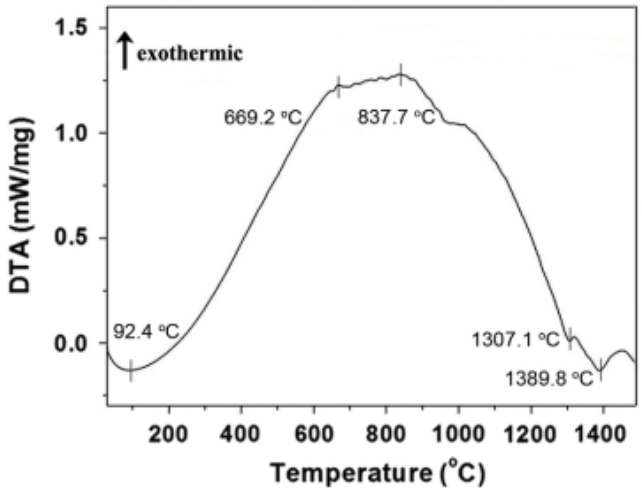

Fig.2.27. *DTA curve of the CoCrFeNiAl HEA powder. [24]*

Figure 2.27 exhibits a thermal analysis result of CoCrFeNiAl HEA powder which is milled for 60 h by DTA curve. The CoCrFeNiAl HEA is manufactured by mechanical alloying. The first endothermic peak occurs at around 92 ^{o}C. Processing controlling agent (PCA) is used to prevent oxidization and cold welding of HEAs. N-heptane is picked to be the PCA which has a bolling point at around 98 ^{o}C. Form 100 ^{o}C, an exothermic curve can be observed. The lattice strain and deformation of structures are the reasons for the release of internal stresses which induce such a exothermic curve. Also, two peaks at 669.2 ^{o}C and 837.7 ^{o}C indicates a phase transformation in the studied material. After 900 ^{o}C, the high temperature introduces the collapse of crystalline structures. This situation can be reflected by the endothermic curve. Finally, two separate endothermic peaks occurs at 1307.1 ^{o}C and 1389.8 ^{o}C from which the melting temperatures of phases can be determined. [24]

2.6 Applications of HEAs

HEAs can be applied in a large amount of applications due to their remarkable properties. Some conventional alloys are replaced by HEAs in many areas in recent years. Although several issues also need to be studied, such as how to reduce the comsumption by manufacturing the HEAs, HEAs can be utilized in the following promising fields:

(1) HEAs can be applied as wear-resistance coatings since their wear resistance and fatigue ratio are higher than those of conventional metallic materials. Such wear-resistance coatings can be utilized on the surface of bearings and jet engine to prevent possible fatigue cracking and abrasive wear during their usages. [25]

(2) HEAs can be utilized as structural materials as they exhibit excellent mechanical properties, like high hardness, high yield strength and high tensile strength. Ideal mechanical properties bring HEAs to certain industrial areas where the requirements of such properties are critical. Nickel alloys and conventional steels can be replaced by HEAs in modern factories and job locations. [25]

(3) In marine engineering, HEAs also play a vital role in resistance to corrosion due to its high corrosion resistance. For example, $Cu_{0.5}$NiAlCoCrFeSi HEA has higher corrosion resistance than that of 304-stainless steel. Tempering processing can improve the corrosion resistance of HEAs.

(4) Ca20Mg20Zn20Sr20Yb20 has been studied as the biodegradable high entropy alloys. After the implantaion, Ca20Mg20Zn20Sr20Yb20 can promote the formation of new bone and will not degrade in a certain duration. In this way, high entropy alloy can be used in biomedical area.

(5) With the concept of high entropy, the fission process of neclear reactors can be simulated. As the nuclear reaction happens, the types of elements increases. Also the potential in resisting irradiation and corrosion makes HEAs the valuable materials in nuclear industries. HEAs can be designed as the protection shell of nuclear equipments. [25]

(6) HEAs can be used as refractory skeleton of buildings due to their high impact resistance and thermostability.

(7) HEAs can be applied in high frequency transformer, coreplane and soft magnetic films.

(8) HEAs provide high wear resistance for a turbine blade. [25]

3 EXPERIMENTS METHODS

In this work, different HEAs were studied to fing out whether the casting methods and manufacturing paramters effect the final microstructures and mechanical properties of HEAs. This project is accomplished by comparing the structures and properties of different high entropy alloys which melted and manufactured in different methods and atomosphere. The reference $Al_{0.5}CrFeCoNiCu$ HEAs were casted after arc-melting for several times. It was provided by Assistant Professor Sheng Guo from Chalmers University of Technology. Meanwhile, the $Al_{0.5}CrFeCoNiCuMo_{0.25}$ and $Al_{0.5}CrFeCoNiCu$ HEAs were casted by induction-melting. After the manufacturing, the samples were cut into small pieces for the follow-on experiments. The microstructures of HEAs were observed by SEM after polishing the samples which fixed in exopy resins. After that, the crystalline structures were characteristized by X-ray diffraction. Finally, the hardness test and compression test were done to evaluate the mechanical properties of HEAs.

3.1 HEA Samples

The arc-melted $Al_{0.5}CrFeCoNiCu$ HEA is chosen as the reference. Also, induction-melted $Al_{0.5}CrFeCoNiCuMo_{0.25}$ and $Al_{0.5}CrFeCoNiCu$ HEAs are casted both in vacuum and air condition. In melting and casting processing of $Al_{0.5}CrFeCoNiCuMo_{0.25}$, molybdenum are added since the molybdenum provides high wear resistance. The final mechanical properties and microstructures are interested since whether the addition of molybdenum will alter the relative properties is under estimated. With the reference sample arc-melted $Al_{0.5}CrFeCoNiCu$ HEA and induction melted $Al_{0.5}CrFeCoNiCu$ HEA, comparison between their final properties will also provides some ideas about how to choose a proper melting methods when facing specific issue. For reference material and induction-melted $Al_{0.5}CrFeCoNiCu$, the composition is same which can be seen in Table.3.1.1. Meanwhile, 7.3 wt.% molybdenum is added in melting processing before the casting of $Al_{0.5}CrFeCoNiCuMo_{0.25}$.

Table 3.1.1. *Composition of HEA samples during casting.*

Compositions	**Al (wt.%)**	**Co (wt.%)**	**Cr (wt.%)**	**Cu (wt.%)**	**Fe (wt.%)**	**Ni (wt.%)**	**Mo (wt.%)**
Ref. $Al_{0.5}CrFeCoNiCu$	4.5	19.5	17.2	21.0	18.5	19.4	0.0
$Al_{0.5}CrFeCoNiCu$	4.5	19.5	17.2	21.0	18.5	19.4	0.0
$Al_{0.5}CrFeCoNiCuMo_{0.25}$	4.1	18.1	15.9	19.5	17.1	18.0	7.3

3.2 Testing methods

To evaluate the structures and mechanical properties of HEAs, the following experiments were carried out. The microstructures of HEAs could be observed firstly by optical microscope and then spotted in details by SEM. Also, with SEM and EDS, the composition distribution could be estimated. In order to verify the crystalline structures, X-ray diffraction was applied. As for the mechanical properties, the hardness test helped to point out the Vickers hardness value while the compression test contributed to the calculation of yield strength of HEAs.

3.2.1 Optical microscopy and scanning electron microscopy

The optical microscopy (OM) images of HEAs were taken by Materials microscope system Leica DM 2500 while the SEM experiments were finished by Scanning electron microscope Zeiss ULTRAplus.

Fig.3.2.1. *Materials microscope system Leica DM 2500 and Scanning electron microscope Zeiss ULTRAplus. [26]*

The microstructures of HEA samples were studied with SEM. Before carrying out the experiments, samples were firstly mounted with epoxy resin. Then the sample surface was polished. Lubrication were used during the polishing in order to reduce the amount of possibly occurred scratches. After etching, the epoxy samples were observed with OM to estimate whether the quality of HEA samples were enough for the processing of SEM. Total five samples were investigated with SEM: the reference sample, air-casted and vacuum-casted induction-melted $Al_{0.5}CrFeCoNiCuMo_{0.25}$, air-casted and vacuum-casted induction-melted $Al_{0.5}CrFeCoNiCu$. During the SEM lab, HEA samples were observed under different magnifications. Also two different detectors, secondary electron (SE) and angle selective

backscatter (AsB) were utilized to show different contrast. The accelerating voltage was 20 kV (As the figure shows EHT = 20 kV, where EHT refers to electron high tension). Meanwhile the working distance was at arount 8.5 mm.

During the SEM processing, magnification, brightness and contrast need to be adjusted to obtain high contrast images. After imaging the HEA samples, EDS-mapping (Energy-dispersive X-ray spectroscopy mapping) can be obtained using INCA program. EDS (Energy-dispersive X-ray spectroscopy) elemental mapping is a useful tool for determining the elemental distribution in the microstructures of HEAs. The interation between X-ray and sample contributes to the EDS analysis. The electrons of inner shell of sample can be excited by incident beam and the ejected. The outer electons fill in the elctron hell created by the ejection of inner electrons. Thus an X-ray released due to the energy difference between inner shell and outer shell. With energy-dispersive spectrometer, the emitted X-rays can be collected and measured. Since the energies of X-rays are characteristic, different elements can be determined by observing and indexing the positions of peaks from EDS spectrum. Also, an EDS mapping contains different elements can be obtained during this procedure. The obtained 2D picture shows the spatial distribution of each elements in a sample. Different colors refers to different elements in the same focused area which help to distinguish diverse elements.

3.2.2 X-ray diffraction

The X-ray diffraction patterns of each sample was determined by PANalytical Empyrean Multipurpose Diffractometer (PANalytical X-ray diffractometers). It could be applied in qualitative and quantitative phase analysis of HEAs. Before the XRD experiment, the samples were polished and etched to expose smooth flats.

Fig.3.2.2. PANalytical Empyrean Multipurpose Diffractometer *[27]*

In XRD processing, the sample was positioned in a sample holder while the detector moved in a circle around the sample. The sample holder was Chi-Phiz stage.The angle 2theta refered to the positions of detector. As to obtain the accurate results, the samples were positioned in a specific height which could be alterd by holder leg with different length. The positions of peaks were measured between 20 to 120 (°2θ). During the processing, the X-rays reached to the sample surface and the diffracted beams were collected by detector. The diffraction fullfills the Bragg's law. Since each diffracted beam is characteristic, distinct phases and crystalline structures could be determined by X-ray diffraction.

3.2.3 Hardness testing

Mechanical properties of HEAs were also interested since these parameters help to evaluate whether a specific type of HEA could be applied in industrial areas or not.

For hardness test of HEAs, the widely used method is Vickers hardness test. In this work, Vickers hardness ISP 6507 standard was used. A pyramidal diamond indentor was used as well. This method had a reliable result for very hard materials as the diamond indentor would not deform even at a high loads exerted by a simple weighted lever. After the indenter penatrated into the surface of the sample, an impression square formed. By measuring the length of impression diagonals, the hardness value could be obtained by convertion and calculation. Since the machine automatically deal with these values, a final hardness report could be printed easily. However, some errors induced by surface finish and flatness may happen during the hardness tests. Also, the thickness of sample should be considered since the specimen table may influence the final result when the sample is too thin. [28] In this work, the hardness tester was Duramin-A300 hardness testing system.

The Vickers hardness number can be determined by the ratio F/A where F refers to the applied force and A is the impression area [28]. The equation is as follow:

$$HV = \frac{F}{A} = \frac{0.1819F}{d^2} \text{ [kgf/mm}^2\text{]} \quad (3\text{-}1)$$

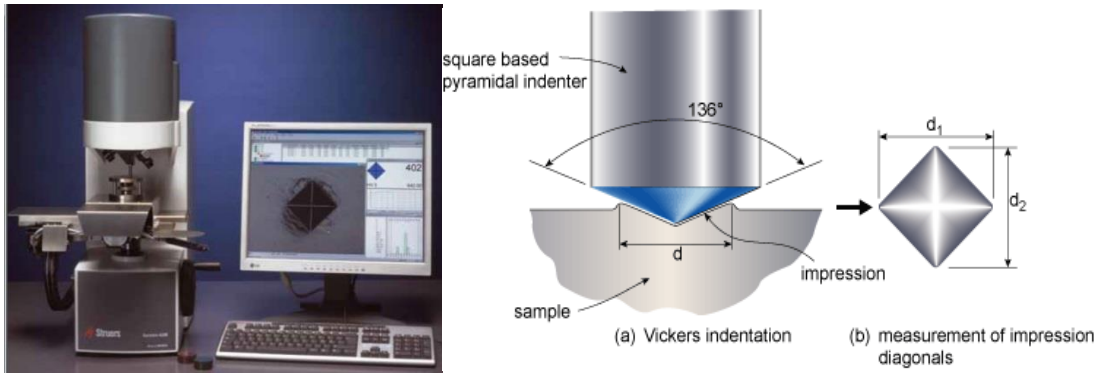

Fig.3.3. *Duramin-A300 hardness testing system and vickers hardness test. [28]*

3.2.4 Compression testing

Compression testing was applied to evaluate the mechanical properties of HEAs and to determine whether the mechanical properties. Both yield strength of ductile material and ultimate strength of brittle material could be determined by this method.

The compression testing was accomplished by Servohydraulic materials testing machine Instron 8800. First of all, the dimension and diameters of samples should be recorded as the length change and area needed to be taken into account when calculating the mechanical properties. After that, the samples were positioned carefully between two sensors to ensure concetric loading. During the experiment, both positions of upper sensor and applied force were recorded. With the obtained data, mechanical parameters could be calculated by the following equations.

Engineering strain: $e = \frac{\Delta L}{L} = \frac{l-L}{L}$ (3-2)

True strain: $\varepsilon = \ln(1 + e)$ (3-3)

Engineering stress: $\sigma_e = \frac{P}{A}$ (3-4)

True stress: $\sigma_{true} = (1 + \varepsilon)(\sigma_e)$ (3-5)

Where L is the length of the cylinder specimen, A refers to the cross-section area of specimen. [29]

Fig.3.4. *Instron 8800. [29]*

The limit of Instron 8800 was 200 kN. For ductile materials, yield points or yield strength could be determined. The yield strength is determined by 0.2% offset point in some cases. But in this experiment, the sensor were not so accurate since the diameters of specimen were

relatively small. As to get the accurate results, the yield strength was determined by 5% offset points. Before yield points, the materials deformed elastically and had the ability to go back to their original shapes after removing the applied force. By contrast, as the compression continued after yield points, the materials deformed plastically and endured irreversible deformation. For brittle materials, an uniaxial compression strength could be evaluated. Some brittle materials broke sharply with few deformation or even no deformation. [29]

4 RESULTS AND DISCUSSION

With optical microscope and scanning electron microscope, microstructures of HEAs could be observed. Both dendrite and interdendrite regions could be seen with different magnifications. Also EDS maps were used to evaluate the composition distribution of HEAs. After that, X-ray diffraction was applied to characterize the crystalline structures of HEAs. With that, it could be defined that whether the HEA was in bcc or fcc structure. Finally, hardness test and compression test were carried out to test the mechanical properties of HEAs.

4.1 Optical microscopy images

Optical micrographs could be used to observe microstructure of HEAs. With different magnifications, both overview and details of microstructures could be observed by optical microscope.

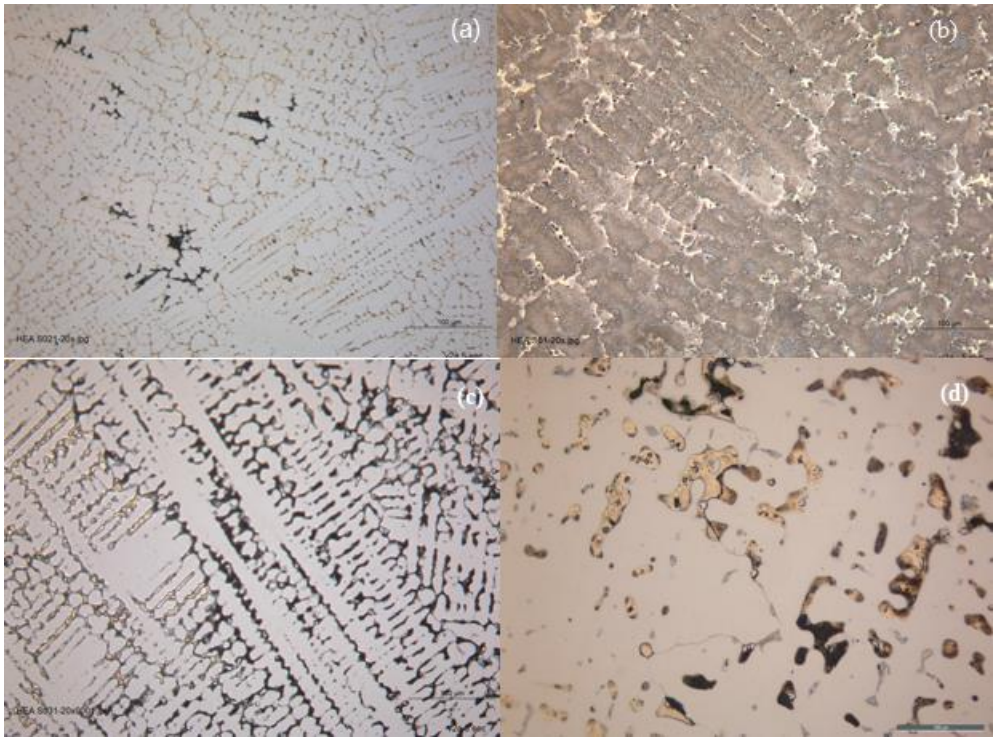

Fig.4.1.1 *Optical microscopy images of (a) reference sample (b) air-casted $Al_{0.5}CrFeCoNiCu$ HEA (c) air-casted $Al_{0.5}CrFeCoNiCuMo_{0.25}$ HEA (d) vacuum-casted $Al_{0.5}CrFeCoNiCu$ HEA (all images are in 20× magnification)*

Figure 4.1.1 gives a basic overview of microstructures of HEAs. The figures are in the same magnification (20×) where the scale bar refers to 100 µm. According to Fig.4.1.1 (a) and

Fig.4.1.1 (a), reference samples and air-casted $Al_{0.5}CrFeCoNiCuMo_{0.25}$ have similar microstructures. The grains are dendrite-like and oriented in all directions. Whitin these two images, bright area represents the dendrite regions while the dark area refers to interdendrite regions. Fig.4.1.1 (b) and Fig.4.1.1 (d) shows the microstructures of $Al_{0.5}CrFeCoNiCu$ which are different from previous described one. The grains are dendrite-like and have larger grain size compared to the size of air-casted $Al_{0.5}CrFeCoNiCuMo_{0.25.}$ Also the interdendrite regions are not so uniform. Futher discussion about microstructures will given by the following SEM images.

4.2 SEM images

During the SEM lab, HEA samples are observed under different magnifications, the scale bar are indicated in the following SEM images. The SEM images of reference material are shown in Fig.4.2.1 with different magnification. The uniform dendrite structures can be observed on the surface while the grains are aligned in different orientation. In Fig.4.2.1, significant contrast of different areas refers to different regions. The pale grey areas refers to dendritic regions. By contrast, the deep color areas represent the interdentritic regions. The dendrite arm sapcing is at around 100 μm. Dendrite arm spacing is the distance between dendrites secondary arms which is also called DAS. Measuring the DAS within SEM images help to explain the mechanical properties of HEAs. Basically, the higher DAS leads to lower yield strength and ultimate tensile strength but has little influence on elongation and hardness of HEAs.

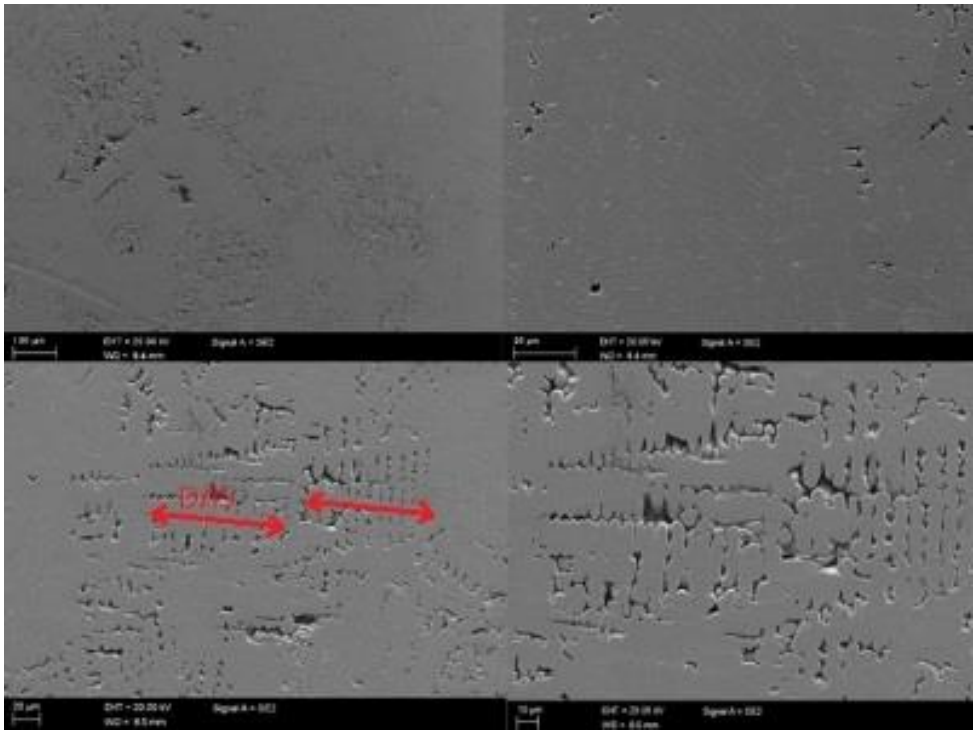

Fig.4.2.1 *SEM images of reference sample.*

From Fig.4.2.2, it can be seen that the air-casted $Al_{0.5}CrFeCoNiCu$ HEA shows dendrite structures also. The alignment of interdendrite regions and dendrite regions are uniform where also some pores and tiny precipates can be observed. The dominant regions in dark color refers to dendrite regions while the minor regions in bright color represent interdendrite regions. The distribution of elements in these two regions will be estimated in EDS mapping.

Fig 4.2.3 shows the SEM images of vacuum-casted $Al_{0.5}CrFeCoNiCu$ HEAs in diverse magnifications. Unlike the previous images, the interdendrite regions behave dendrite-like structures and aligned mainly in vertical orientation. Compared to Fig. 4.2.2, the areas of interdendrite regions are compressed and behave more dispersed.

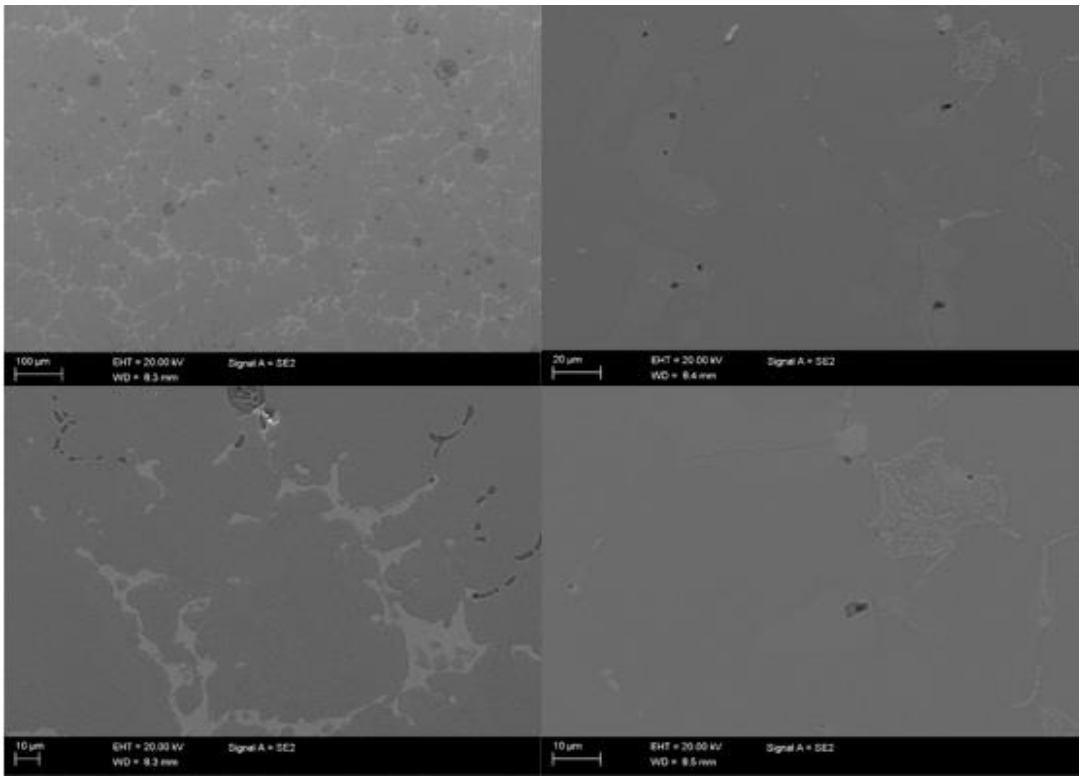

Fig.4.2.2. *SEM images of air-casted $Al_{0.5}CrFeCoNiCu$ HEA.*

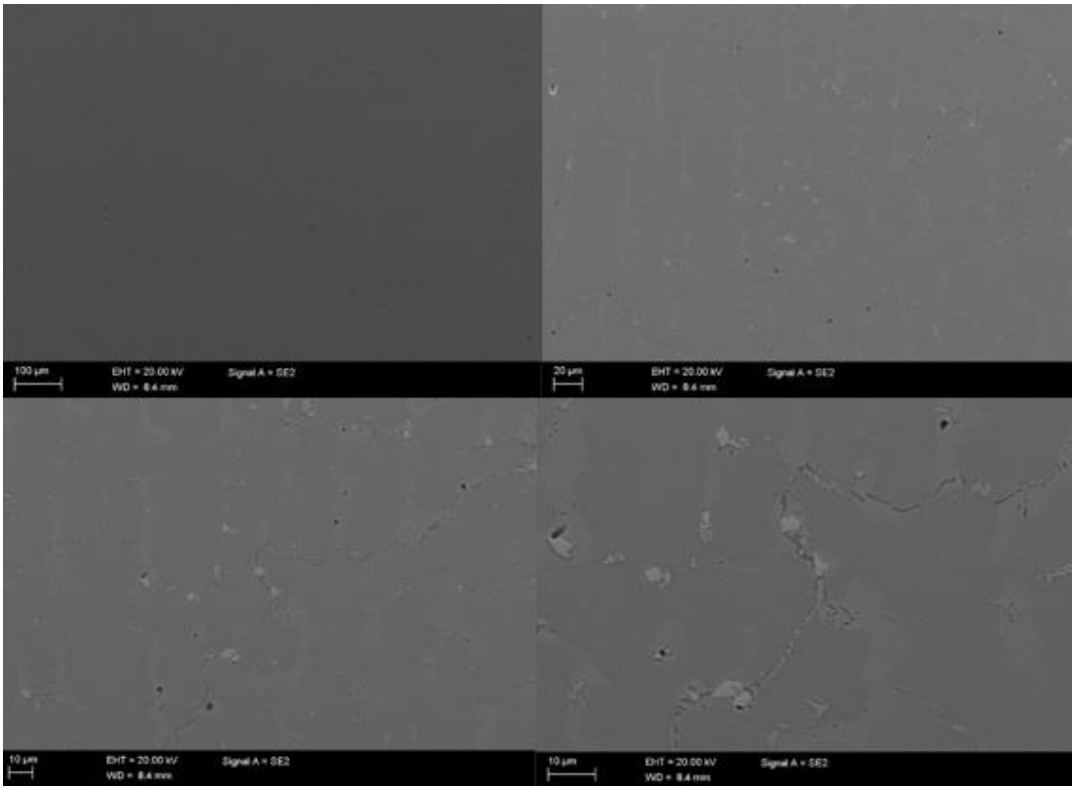

Fig.4.2.3. *Vacuum-casted $Al_{0.5}CrFeCoNiCu$ HEA images taken with SE signal.*

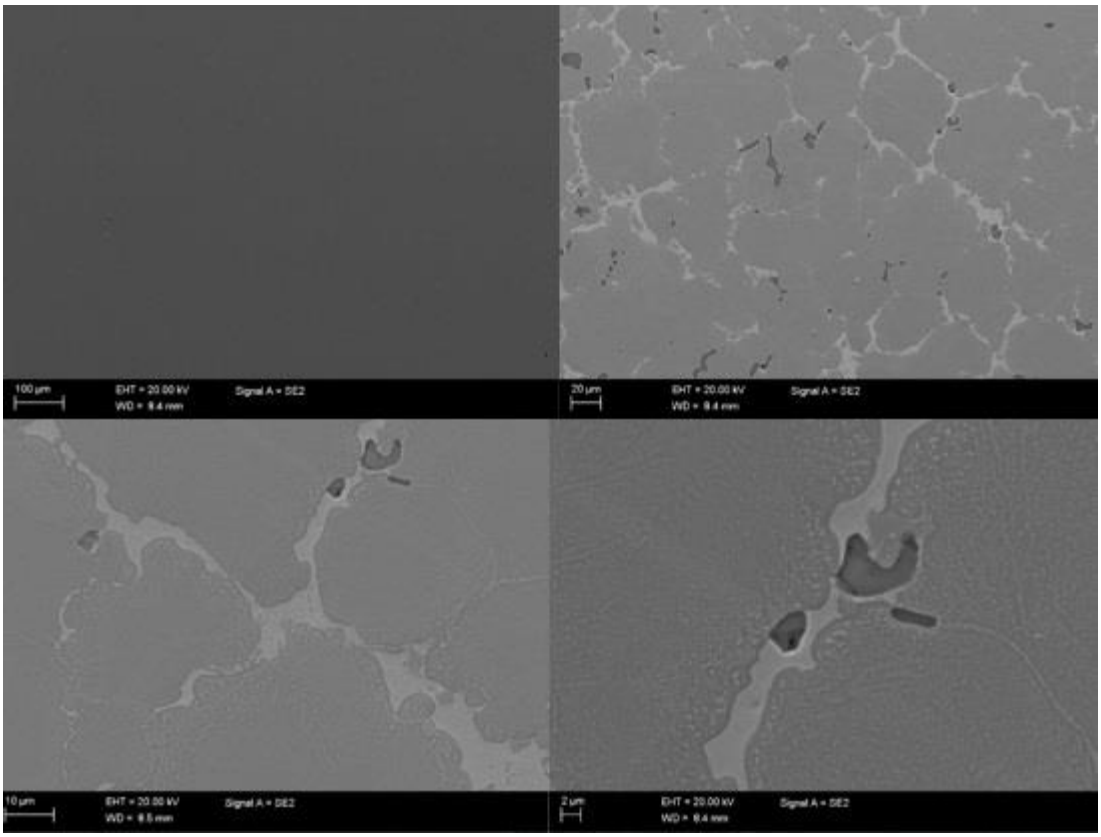

Fig.4.2.4. *SEM images of air-casted $Al_{0.5}CrFeCoNiCuMo_{0.25}$.*

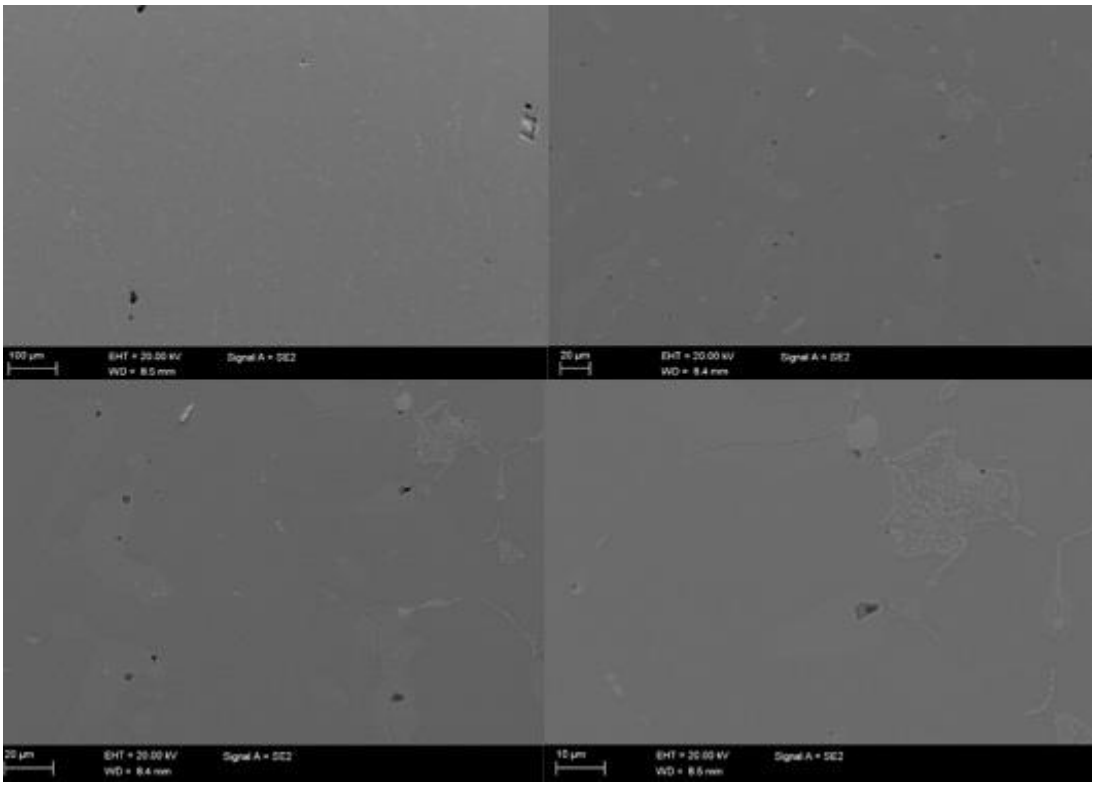

Fig.4.2.5. *SEM images of vacuum-casted $Al_{0.5}CrFeCoNiCuMo_{0.25}$ HEA.*

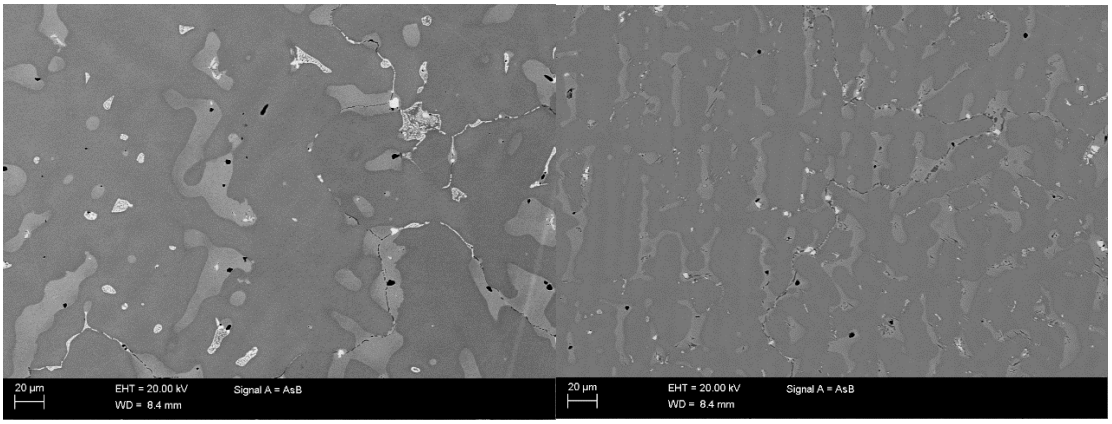

Fig.4.2.6. *Comparison of air-casted (left image) and vacuum-casted (right image) $Al_{0.5}CrFeCoNiCuMo_{0.25}$ HEA images taken with AsB signal.*

The air-casted and the vacuum-casted $Al_{0.5}CrFeCoNiCuMo_{0.25}$ samples both show dendrite-like structures. While the larger area of interdendrite regions are found in air-casted sample. The high vacuum level helps to refine the structure and contributes to the formation of small grain sizes. In both SEM images, dark spots are observed in dendrite regions and interdendrite regions which refer to the molybdenum containing phases and sulfur impurities.

4.3 EDS mapping

EDS mapping gives information about the distribution of a alloy sample elements. Fig.4.3.1 presents the EDS map of reference sample. From the EDS map, the cobalt, chromium and iron are mainly located in the dendrite regions. By contrast, copper mainly gathered in the interdendrite regions. Meanwhile, alumnium and nickel have the uniform distribution among these two regions. The data in Table.4.3.1 also gives the ideas that the interdendrite regions mainly consists of copper containing substance (approximately 50 wt.% Cu) On the opposite side, the dendrite regions contains a large amount of nickel, chromium, cobalt and iron cotaining phases and a small amount of alumnium containing phase. As for the air-casted and vacuum casted $Al_{0.5}CrFeCoNiCu$ samples, the distribution of each elements in different regions is no significant diffenerce to that of reference one except for the size of dendrite regions.

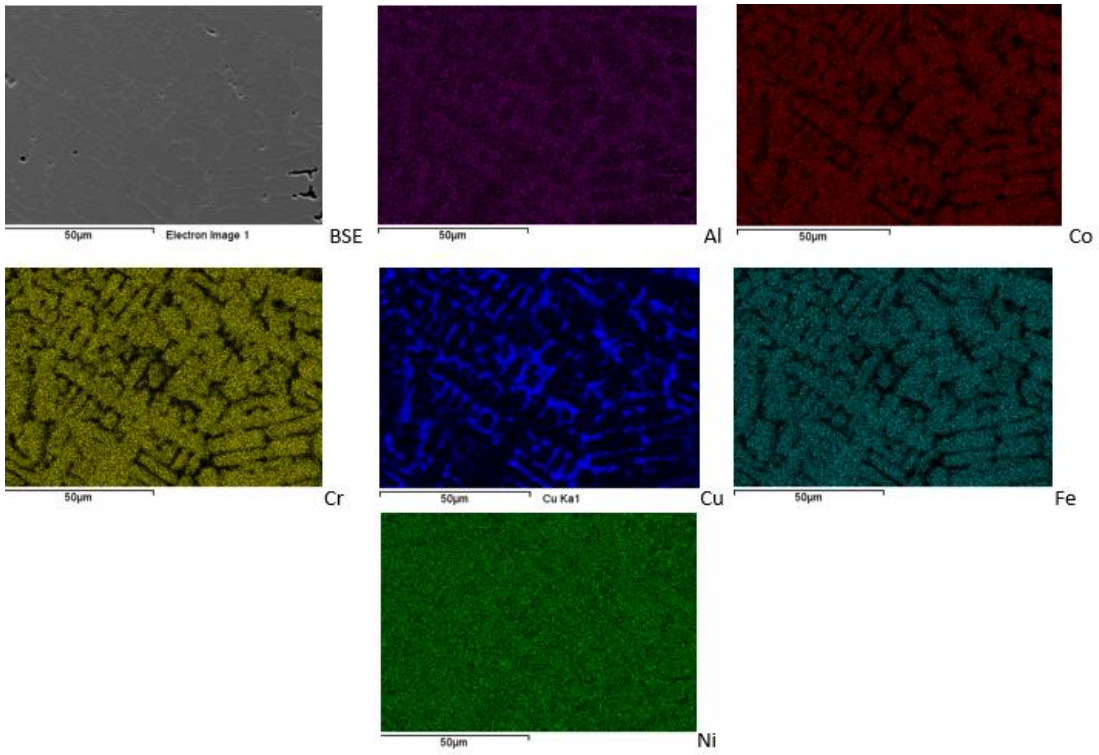

Fig.4.3.1. *EDS mapping of reference sample.*

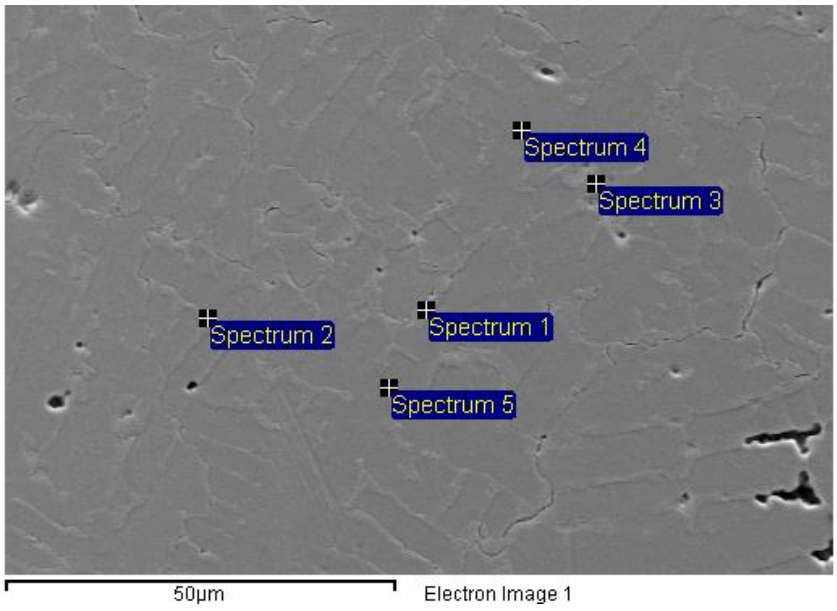

Fig.4.3.2. *EDS mapping of reference sample.*

Table 4.3.1. *Alloying element measured in Fig.4.3.2.*

Spectrum	Al (wt.%)	Cr (wt.%)	Fe (wt.%)	Co (wt.%)	Ni (wt.%)	Cu (wt.%)
Spectrum 1	6.4	8.7	9.3	14.4	17.6	43.6
Spectrum 1	6.5	7.9	6.9	6.8	13.9	58.0
Spectrum 1	4.9	17.8	17.6	26.7	19.2	13.8
Spectrum 1	3.0	19.8	20.5	31.1	16.1	9.4
Spectrum 1	2.9	20.1	21.0	31.4	15,7	9.0

In the EDS mapping of $Al_{0.5}CrFeCoNiCu$ (Fig.4.3.3), the dendrite regions have larger area compared to the reference sample. Meanwhile, apart form the basic metallic elements, a contamination of sulfur is also found in EDS mapping which is mainly located in dendrite region. In Fig.4.3.3, cobalt, iron and chromium phases gather in dendrite regions while copper mainly locates in interdendrite regions. There is no significant difference of composition distribution between induction-melted $Al_{0.5}CrFeCoNiCu$ and reference one apart from the sulfur impurity.

Since the $Al_{0.5}CrFeCoNiCuMo_{0.25}$ sample contains molybdenum also, the EDS maps are also plotted to observe the location of molybdenum phases by Fig.4.3.4. Similar to previous cases, cobalt, iron and chromium mainly exist in dendrite regions while copper locates in interdendrite regions. Besides, a new regions which is indicated in the right upper part of Fig.4.3.4 occurs. The molybdenum containing phase and sulfur contamitation are obseserved in this region. Besides, molybdenum can also be seen in the dendrite regions. However, the aluminum only exists in a small spot in EDS mapping which may reflect the loss of aluminum during the air-casting. The loss of aluminum is a consequence of oxidation reaction.

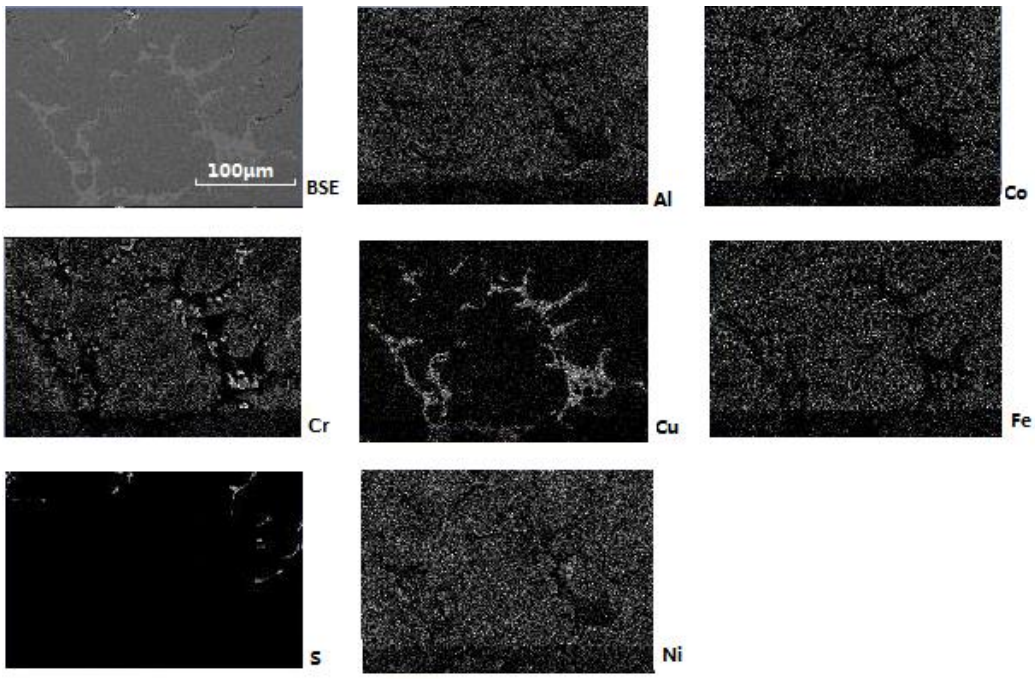

Fig.4.3.3. *EDS mapping of air casted* $Al_{0.5}CrFeCoNiCu$ HEA.

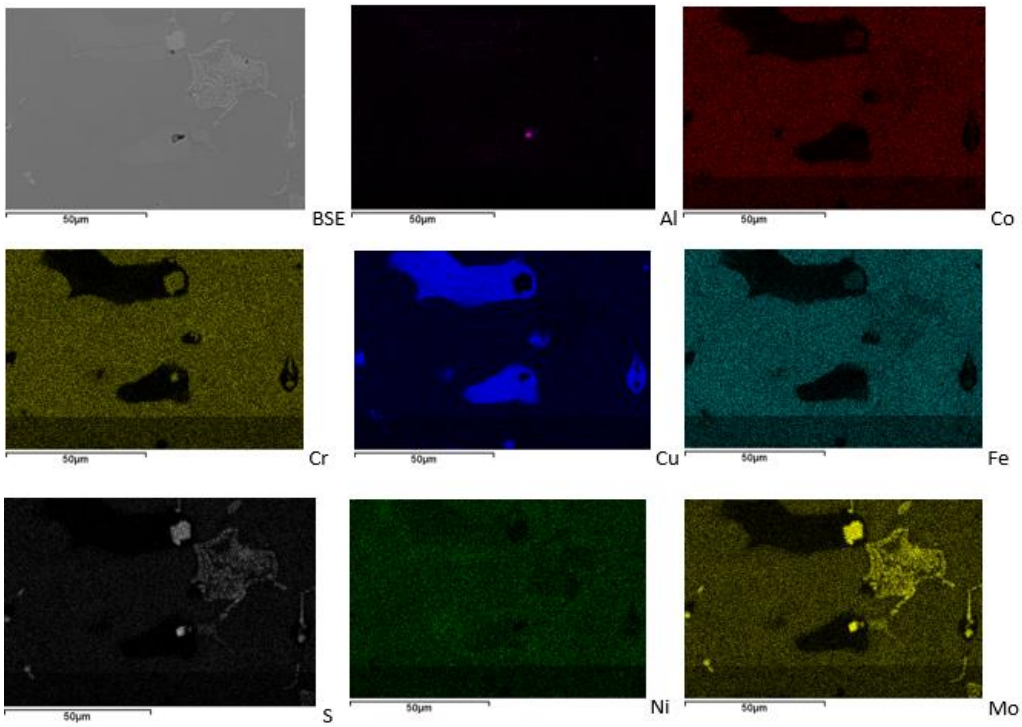

Fig.4.3.4. *EDS mapping of air casted* $Al_{0.5}CrFeCoNiCuMo_{0.25}$ HEA.

4.4 X-ray diffraction

The crystal structures of HEAs samples were characterised by X-ray diffraction. The dominant phases were evaluated by comparing the positions and indensities of peaks from XRD patterns with a reference card.

HEA reference samples had a fcc structure which showed in Fig.4.1.1. The dominant phases were copper nickel (indicates by blue line) and copper iron (pink line). The highest peak existed at 43.50° which refered to fcc (1, 1, 1) plane, other peaks represented fcc (2, 0, 0) plane, fcc (2, 2, 0) plane, fcc (3, 1, 1) plane and fcc (2, 2, 2) plane. From XRD pattern, it can be concluded the reference material is fcc structure.

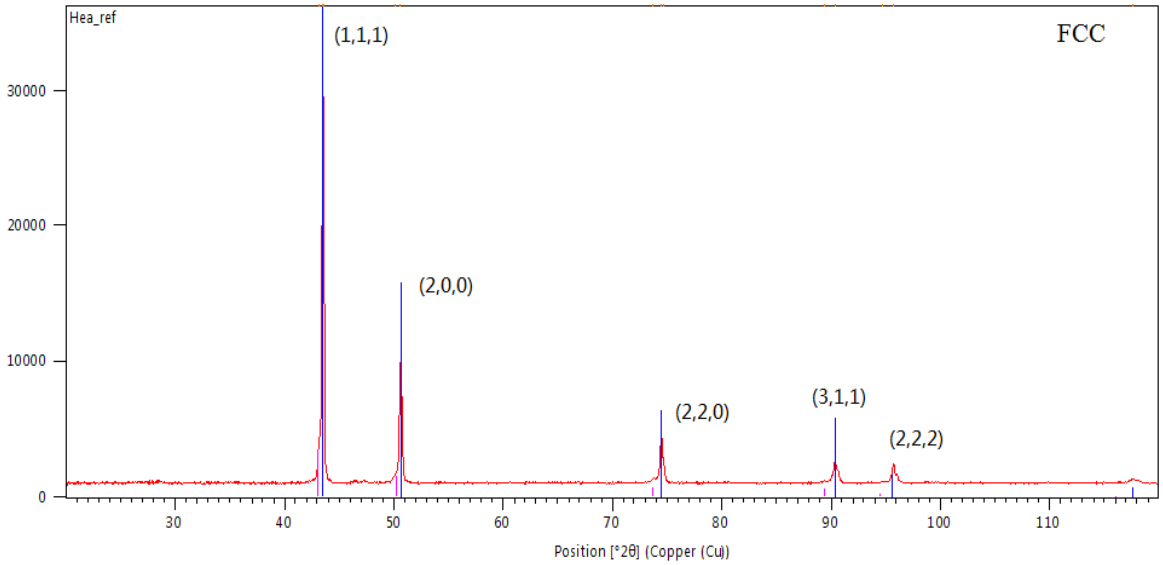

Fig.4.4.1 *HEA reference*

Although induction-casted $Al_{0.5}CrFeCoNiCu$ HEA samples had the same composition as reference samples during casting, the crystal structures were different. Both the air-casted $Al_{0.5}CrFeCoNiCu$ HEA sample and vacuum-casted $Al_{0.5}CrFeCoNiCu$ HEA samples were dual-phase structures which means both bcc-structure and fcc-structure could be found in this material. For the air-casted $Al_{0.5}CrFeCoNiCu$ sample, the highest peak was positioned at 44.55° (2θ) which had the height as high as 27431.84 (counts). That peak refered to bcc (1, 1, 0) plane. However, also fcc(2, 2, 0) plane and fcc (2, 2, 0) plane could be found in XRD of $Al_{0.5}CrFeCoNiCu$ HEA. So it is said that $Al_{0.5}CrFeCoNiCu$ HEA had a mixed fcc + bcc structure. The dominant phases showed in Fig 4.4.2 are aluminum chromium cobalt iron nickel ($Al_{0.4}Cr_{0.4}Co_{0.4}Fe_{0.4}Ni_{0.4}$) and aluminum copper. As for the vacuum-casted $Al_{0.5}CrFeCoNiCu$ HEA, the highest peak existed at 44.50° (2θ) and the pattern was alike but

not totally similar to that of air-casted $Al_{0.5}CrFeCoNiCu$ HEA. The dominant phases were aluminum chromium cobalt and iron nickel. Normally, the fcc structure will be more ductile than bcc structure as the bcc lattice is not closely packed and thus forms brittle and hard phases.

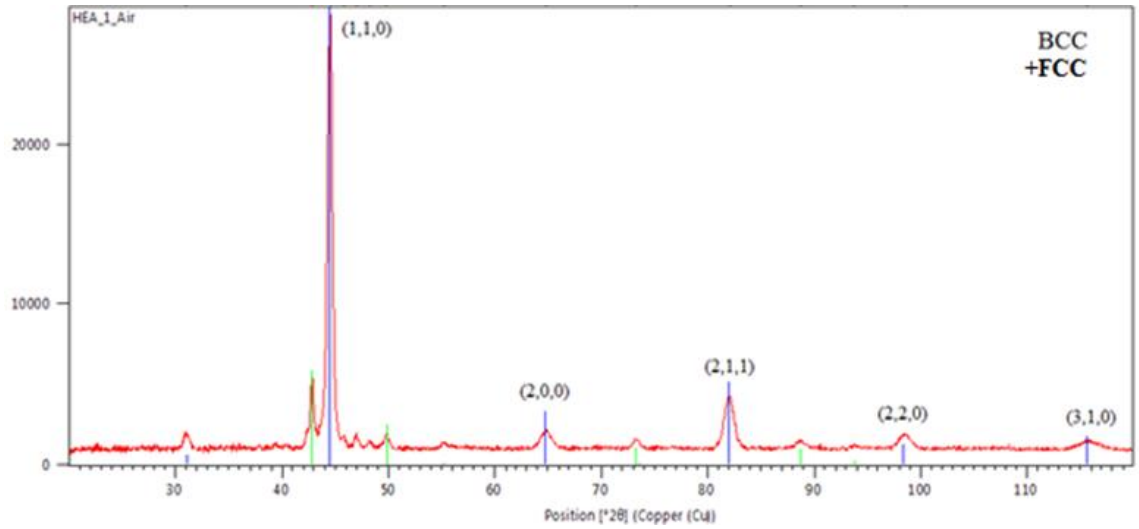

Fig.4.4.2 *XRD of air-casted $Al_{0.5}CrFeCoNiCu$ HEA*

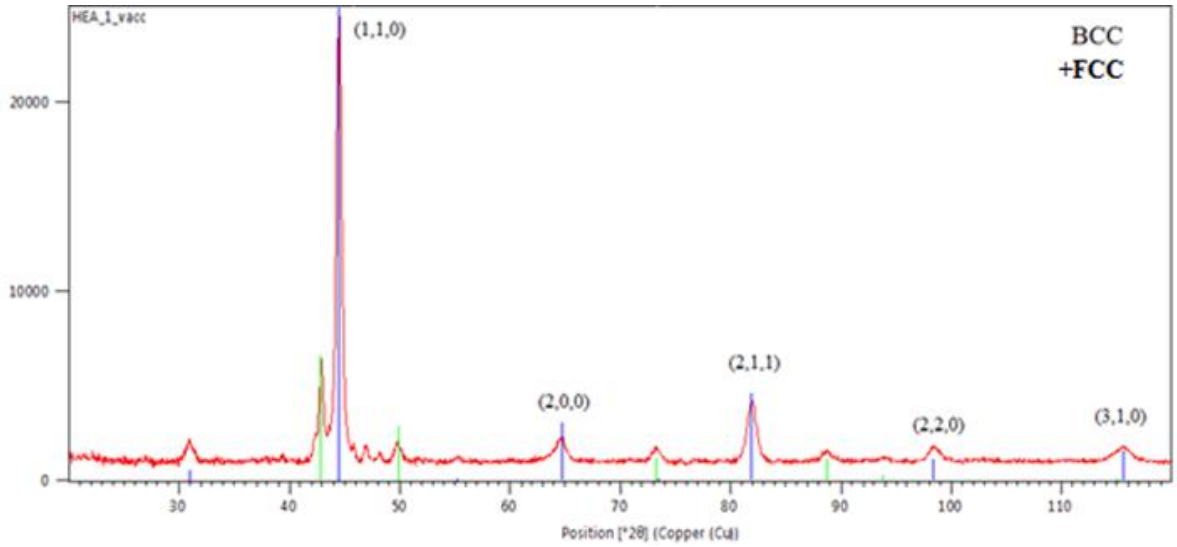

Fig.4.4.3 *XRD of vacuum-casted $Al_{0.5}CrFeCoNiCu$ HEA*

Surprisingly, in Fig.4.4.4 and Fig.4.4.5, it could be seen that $Al_{0.5}CrFeCoNiCuMo_{0.25}$ HEA samples had the similar structures with reference samples even they had different compositions. The main phases were $Mo_{0.27}Ni_{0.73}$ and $Cu_{0.8}Fe_{0.2}$ both in air-casted and

vacuum-casted $Al_{0.5}CrFeCoNiCuMo_{0.25}$ HEA samples. These two samples also behaved fcc structure where also a small peak of fcc (4, 0, 0) plane could be observed.

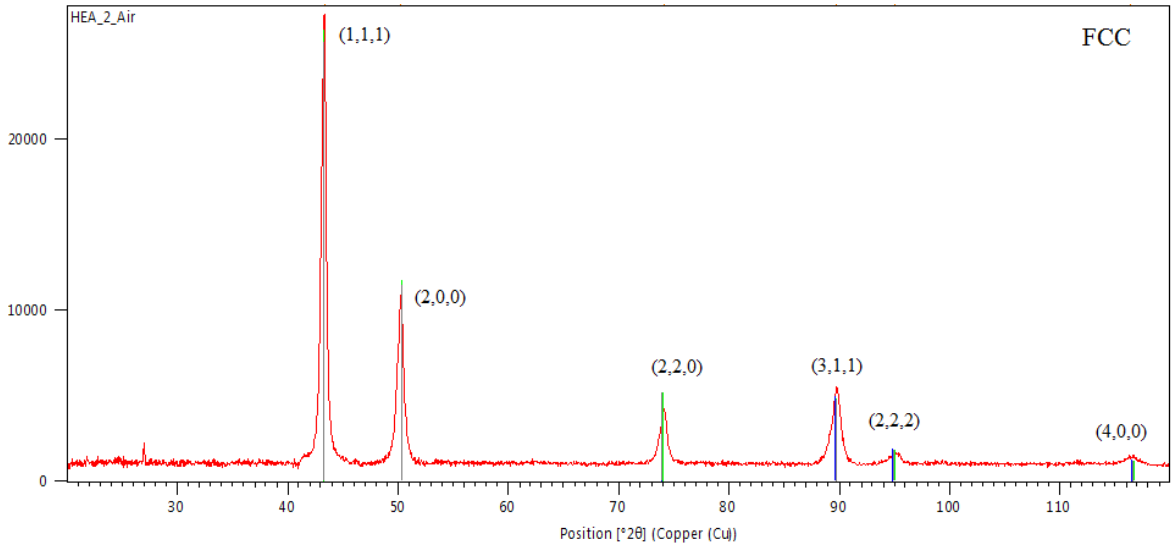

Fig.4.4.4 *XRD of air-casted $Al_{0.5}CrFeCoNiCuMo_{0.25}$ HEA*

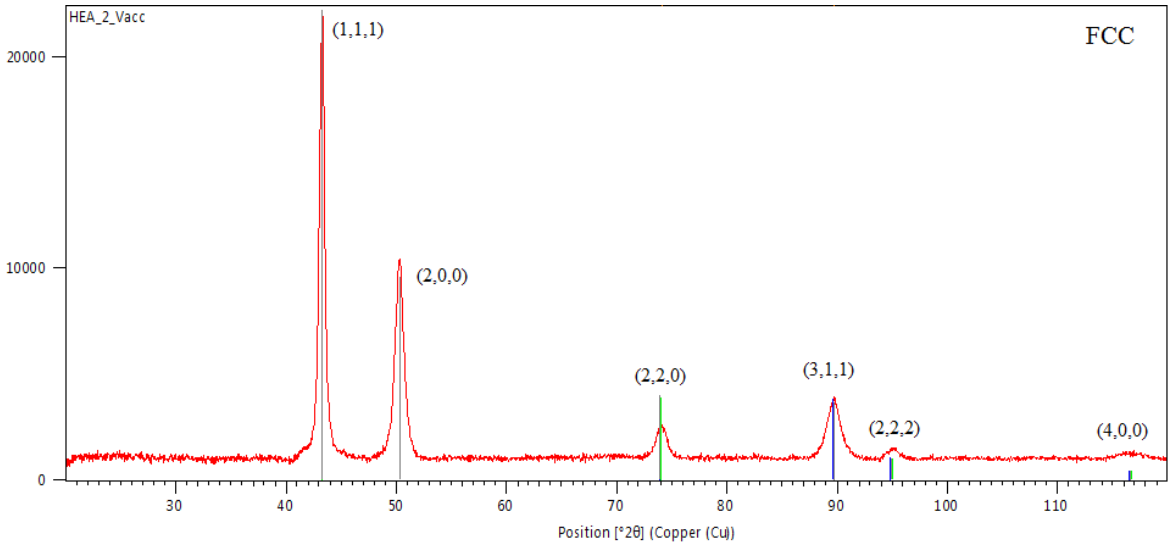

Fig.4.4.5 *XRD of vacuum-casted $Al_{0.5}CrFeCoNiCuMo_{0.25}$ HEA*

In summary, a fcc + bcc dual phase can be found in induction-melted $Al_{0.5}CrFeCoNiCu$ HEA. Meanwhile in reference and $Al_{0.5}CrFeCoNiCuMo_{0.25}$ HEAs, only fcc structure can be observed. The cooling rate may be the reasons for different crystalline structures. As the cooling rate increases, the severer sluggish diffusion effect induces a more simple phase by

limiting the growing space of grains, thus it prefers to form bcc or fcc structure respectively instead of a dual phase consists of fcc + bcc structure.

4.5 Hardness test

The following figures represents the Vikers hardness value of each samples. The average hardness value of reference sample is 189.4 HV. Meanwhile, the air-casted $Al_{0.5}CrFeCoNiCu$ has the similar hardness compared to the reference one, which is approximately 189.9 HV. However, the hardness inceases dramatically when casting the $Al_{0.5}CrFeCoNiCu$ in vacuum condition. The final product has the hardness as high as 551.6 HV. The reasons for such a high hardness may attributes to the formation of mixed phase which contains sulfur impurities.

As for the air-casted and vacuum-casted $Al_{0.5}CrFeCoNiCuMo_{0.25}$, the hardness value remains in the same level, which is 237.8 HV and 240.5 HV respectively. The indcution-melted $Al_{0.5}CrFeCoNiCuMo_{0.25}$ had higher hardness than reference one. The reason for it may be the addition of molybdenum since molybdenum has higher hardness than other added metallic elements. since molybdenum This result provide a idea about the induction-melted $Al_{0.5}CrFeCoNiCu$ samples may not suitable for application since the hardness value is not stable in different casting atomosphere.

Pointnr.	Hardness	Diameter
1	186	172,7
2	182	174,7
3	188	172,1
4	178	176,5
5	197	167,9
6	199	167,3
7	195	169,1

Fig.4.5.1. *The hardness values of reference sample.*

Pointnr.	Hardness	Diameter
1	188	171,9
2	192	170,1
3	184	173,9
4	195	168,7
5	190	170,9

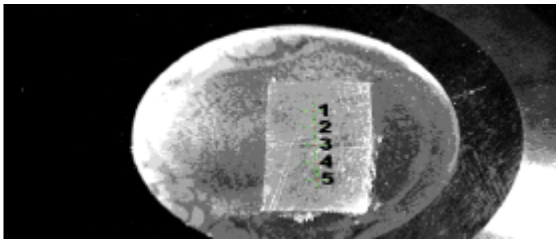

Fig.4.5.2. *The hardness values of air-casted $Al_{0.5}CrFeCoNiCu$.*

Pointnr.	Hardness	Diameter
1	243	151,2
2	244	151,0
3	239	152,6
4	232	154,9
5	248	149,8
6	225	157,3
7	234	154,1

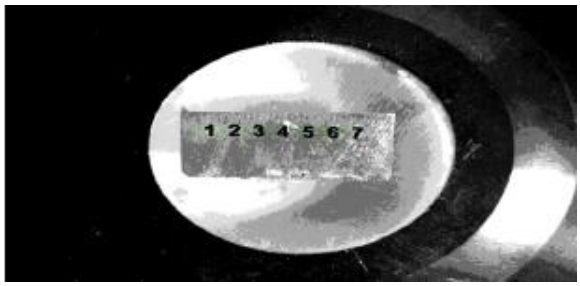

Fig.4.5.3. *The hardness values of air-casted Al0.5CrFeCoNiCuMo0.25.*

Pointnr.	Hardness	Diameter
1	552	100,4
2	556	100,0
3	586	97,4
4	534	102,0
5	543	101,2
6	536	101,8
7	554	100,2

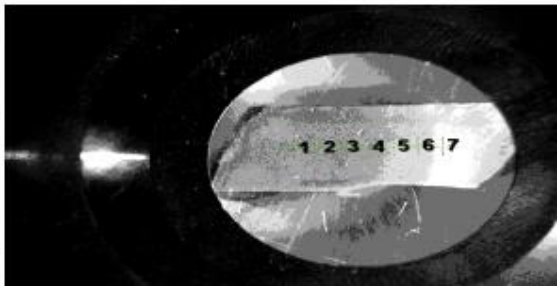

Fig.4.5.4. *The hardness values of vacuum-casted $Al_{0.5}$CrFeCoNiCu.*

Pointnr.	Hardness	Diameter
1	246	150,2
2	220	159,1
3	245	150,6
4	238	152,8
5	243	151,4
6	239	152,4
7	253	148,2

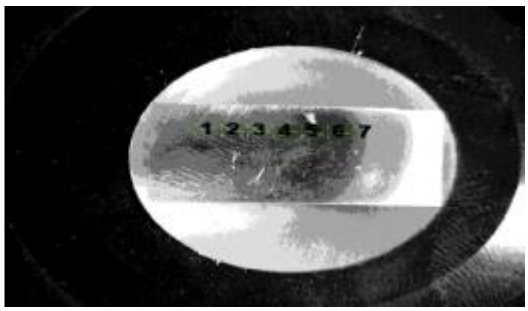

Fig.4.5.5. *The hardness values of vacuum-casted $Al_{0.5}$CrFeCoNiCu$Mo_{0.25}$.*

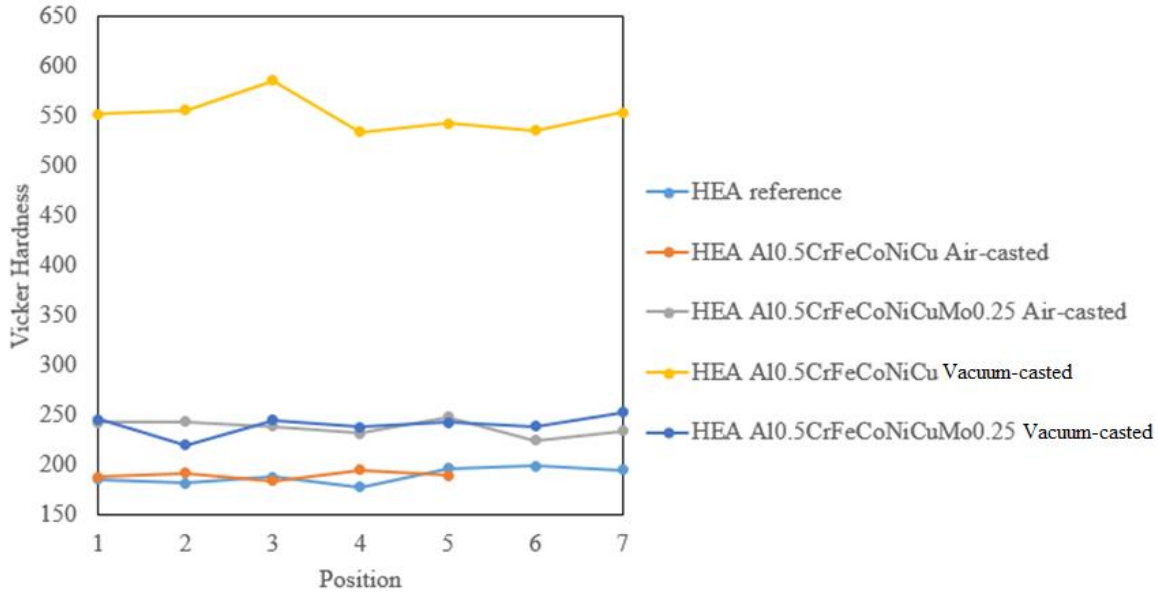

Fig.4.5.6. *Comparison of hardness of different samples.*

4.6 Compression tests

The compression test of HEAs samples were carried out with different testing speeds. For reference samples, since the diameter and length was relatively small (the diameters of each sample are presented in Table.4.6), the tesing speeds were selected as 0.3 mm/s and 0.003 mm/s. Meanwhile, the testing speeds for induction-melted samples were 0.8 mm/s and 0.008 mm/s. In first step, the sample was compressed with a testing speed as 0.003 mm/s and the maximum load was 20 kN. After the sample was compressed into small plate, removed it and put another refernce sample in the test fixture and compressed it with a testing speed as 0.3 mm/s. These two steps were set up to see whether the testing speed influences the mechanical behaviours of HEAs. The results were plotted in Fig.4.6.1 and Fig.4.6.2.

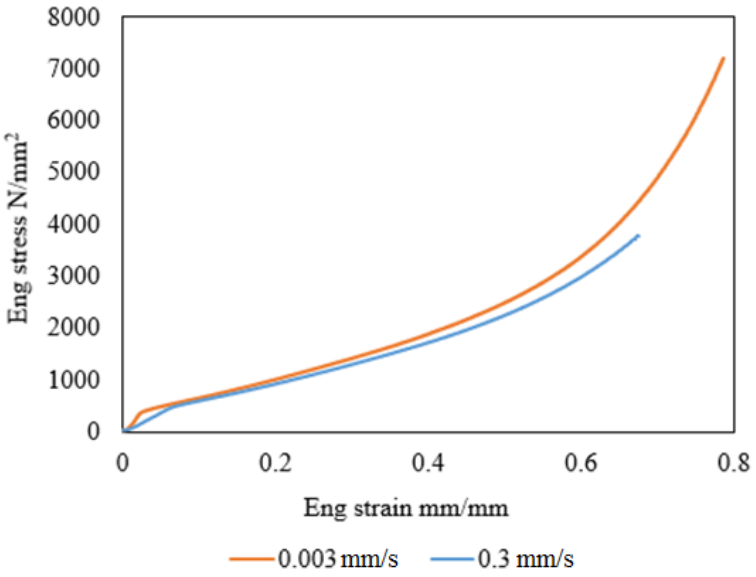

Fig.4.6.1. *Engineering stress vs strain curves of reference samples.*

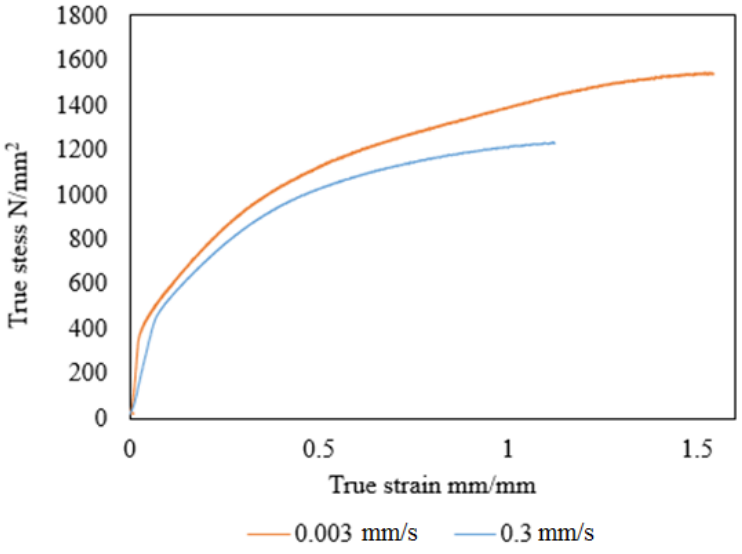

Fig.4.6.2. *True stress vs strain curves of reference samples.*

Fig.4.6.1 and Fig.4.6.2 shows the compression test results of reference samples. From the stress vs strain curves it can be concluded that the reference samples are ductile materials which experience plastic deformation instead of beakage during compression test. Also yield strength could be determined. (See Table.4.6.1) Apparently, the testing speed does not influence the tendency of strain-stress curves but affect the yield strength of materials. The

value for yield point is set at 5% offset point since the data obtained by LVDT sensors is inaccurate.

As for $Al_{0.5}$CrFeCoNiCu HEA samples, the testing speeds were set as 0.8 mm/s and 0.008 mm/s. From Fig.4.6.3 and Fig.4.6.4, it can be defined that the induction-melted $Al_{0.5}$CrFeCoNiCu HEA samples are brittle materials. When compressed the sample in a testing speed of 0.008 mm/s, the sample did not break and even the shape was not changed so much (the strain was lower than 0.09 mm/mm). When changing the testing speed to 0.8 mm/s, the specimen fractured rapidly and broke into pieces. Comparing the different samples, it can be concluded that higher unaixial compression strength can be obtained with lower tesing speed. Besides, there is no significant difference between air-casted samples and vacuum-casted samples when compressed them in a same tesing speed.

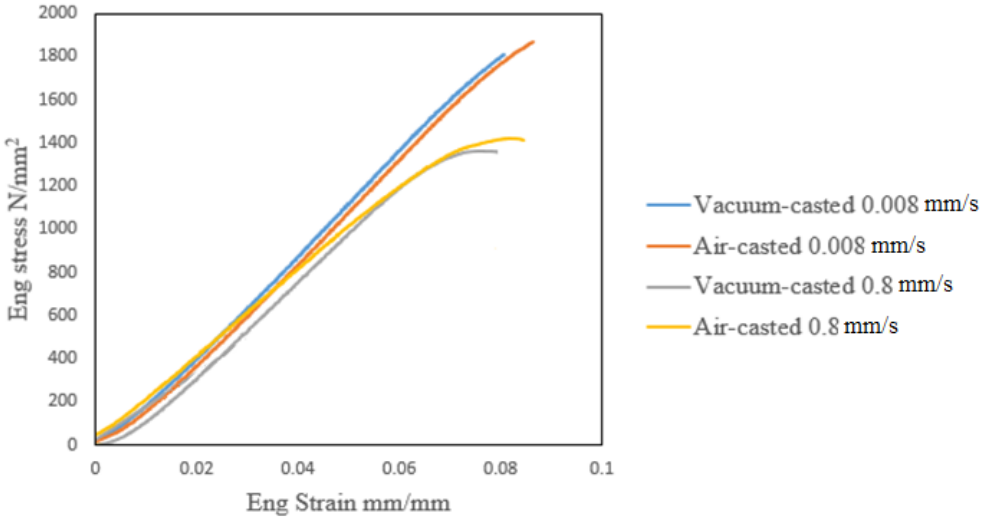

Fig.4.6.3. *Engineering stress vs strain curves of $Al_{0.5}$CrFeCoNiCu HEA samples.*

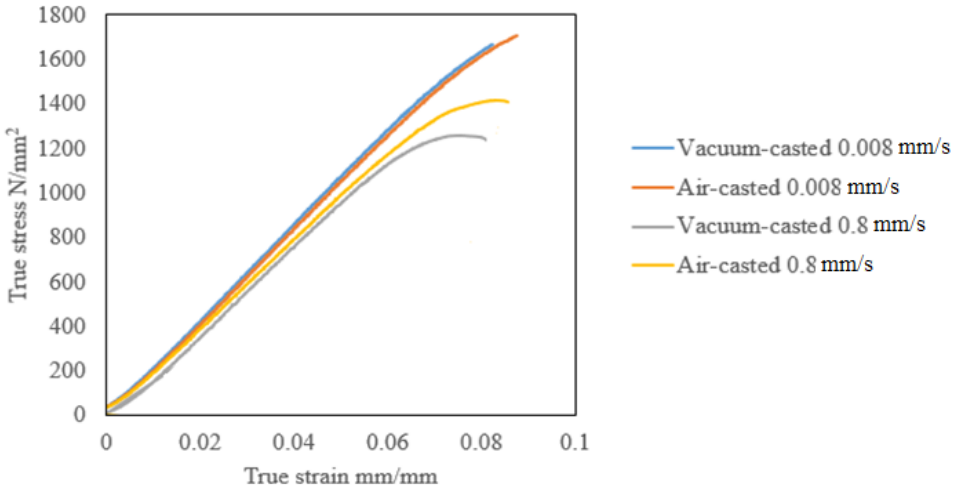

Fig.4.6.4. *True stress vs strain curves of $Al_{0.5}$CrFeCoNiCu HEA samples.*

When considering the $Al_{0.5}$CrFeCoNiCu$Mo_{0.25}$ HEA samples, the materials behaves ductility. When compressed samples in the same tesing speed, the air-casted samples had higher yield strength than that of vacuum-casted one. Genarally, the yield strength increased with the tesing speed. When combined the previous mentioned crystalline structures form XRD patterns, it could be concluded that the fcc-structured reference samples and $Al_{0.5}$CrFeCoNiCu$Mo_{0.25}$ HEA samples were ductile materials and deformed when compressed, the yield strength was increasing with the strain rate. Also the cooling rate has an impact on mechanical properties of HEAs. Higher cooling rate leads to smaller sizes of structures and thus induces higher yield strength. As for the induction-casted $Al_{0.5}$CrFeCoNiCu HEAs, the materials behaves brittle and higher testing speed lead to lower uniaxial compressive strength.

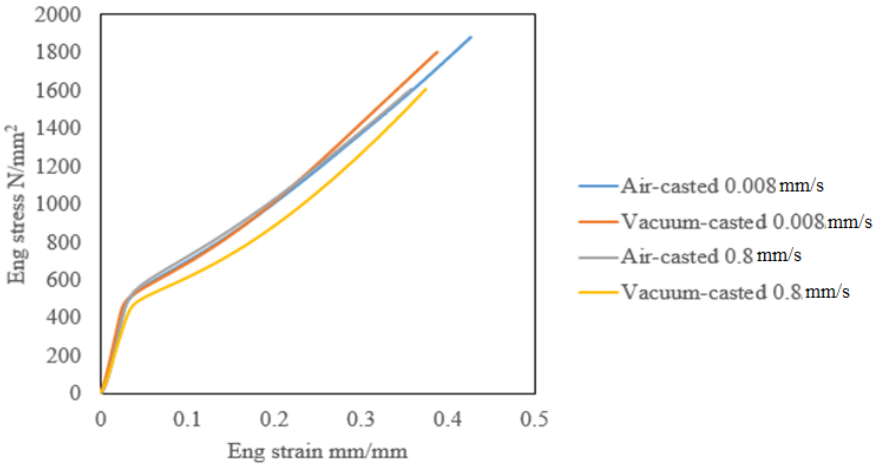

Fig.4.6.5. *Engineering stress vs strain curves of $Al_{0.5}CrFeCoNiCuMo_{0.25}$ HEA samples.*

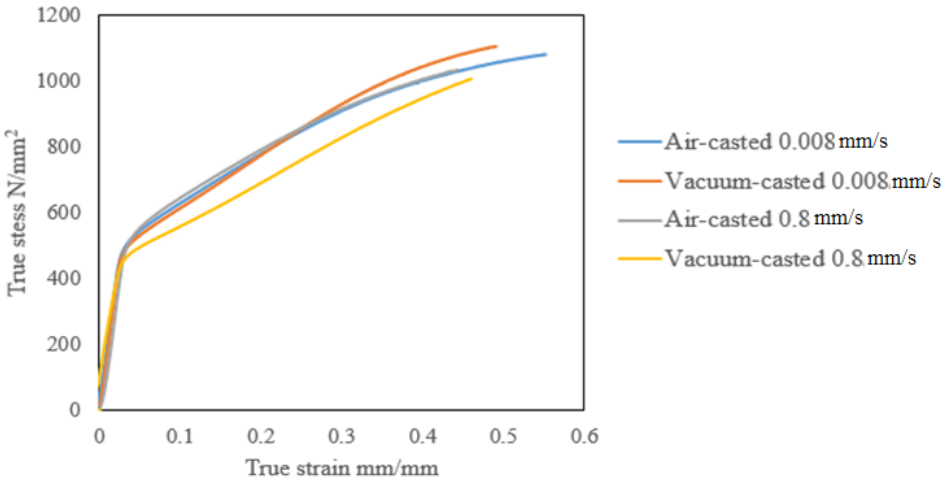

Fig.4.6.6. *True stress vs strain curves of $Al_{0.5}CrFeCoNiCuMo_{0.25}$ HEA samples.*

Table.4.6. *Compression mechanical properties of HEAs*

Sample	Length (mm)	Diameter (mm)	Area (mm^2)	Testing speed (mm/s)	Yield strength (MPa)	Uniaxial compressive strength (MPa)
HEA_ref_10^{-1}	3.00	2.78	6.01	0.3	654.20	-
HEA_ref_10^{-3}	3.15	2.76	5.98	0.003	380.90	-
HEA1_air_10^{-1}	7.85	7.99	50.13	0.8	-	1414.95
HEA1_air_10^{-3}	7.79	7.94	49.51	0.008	-	1705.72
HEA1_vac_10^{-1}	7.84	7.99	50.13	0.8	-	1259.95
HEA1_vac_10^{-3}	7.90	7.96	49.76	0.008	-	1565.14
HEA2_air_10^{-1}	8.02	7.97	49.89	0.8	607.83	-
HEA2_air_10^{-3}	8.07	7.98	50.01	0.008	601.80	-
HEA2_vac_10^{-1}	8.00	7.97	49.89	0.8	525.56	-
HEA2_vac_10^{-3}	7.99	7.98	50.01	0.008	574.79	-

After the compression test, air-casted $Al_{0.5}CrFeCoNiCuMo_{0.25}$ HEA samples were investigated by optical microscope. Fig.4.6.7 compared the microstructures of air-casted $Al_{0.5}CrFeCoNiCuMo_{0.25}$ HEA before and after the compression. The optical microscopy images were taken in the same magnification. It could be seen that the interdendrite regions

deforms heavily. Since the dominant phase in interdendrite regions was copper phase which was soft and ductile, the deformation happened in this region.

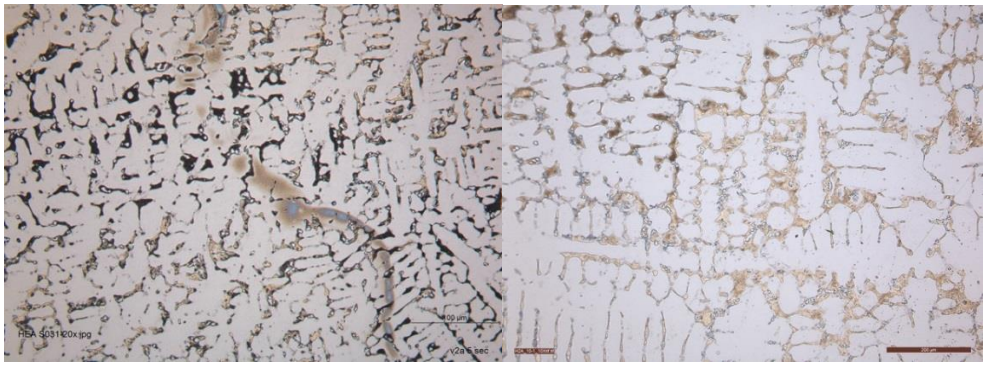

Fig.4.6.7. *Comparison of $Al_{0.5}CrFeCoNiCuMo_{0.25}$ HEA samples (a) Before compression (b) After deformation.*

In summary, by comparing different microstructures of HEA specimens, it could be seen that the induction-melted samples had lager grain sizes than that of reference samples. Also, larger dendrite and interdendrite regions were found in air-casted induction-melted SEM micrographs. Besides, sulfur contamination is found in induction-melted samples. Sulfur contamination have adverse effect on oxidation resistance and the stress-rupture life of HEAs. Hence, arc-melting processing with higher cooling rates and higher vacuum level are recommended since they contribute to refine the structures and form smaller grain sizes of HEAs.

By XRD, the crystalline structures of HEAs were characterized. Both reference samples and induction-melted $Al_{0.5}CrFeCoNiCuMo_{0.25}$ HEA samples were fcc-structured. However, the induction-melted $Al_{0.5}CrFeCoNiCu$ HEA samples were fcc + bcc structured. The cooling rate may be the reason for the different crystalline structures of arc-melted and induction-melted $Al_{0.5}CrFeCoNiCu$ HEA. Higher cooling rate induced the severe sluggish diffusion effect which restricts the growing space of grains thus form a simple structure rather than a dual phase structure.

As for mechanical properties, induction-melted $Al_{0.5}CrFeCoNiCu$ HEA had higher hardness and showed brittle compared to reference specimens. Besides, the $Al_{0.5}CrFeCoNiCu$ HEA casted in vacuum had extreme high hardness. Both fcc-structured reference samples and induction-melted $Al_{0.5}CrFeCoNiCuMo_{0.25}$ HEA samples showed ductility whereas induction-melted $Al_{0.5}CrFeCoNiCu$ HEA samples were brittle and rigid. The larger grain size and mixed bcc + fcc structure made the induction-melted $Al_{0.5}CrFeCoNiCu$ HEA samples

hard and brittle. By contrast, smaller grain sizes and fcc structure induced by higher cooling rate and arc-melting processing made the reference samples soft and ductile. In order to get fine and uniform structure and high mechanical performance, it is recommended to apply arc-melting with a high cooling rate.

5 CONCLUSION

In this work, the main aim to determine whether induction-melted HEAs show similar structures and mechanical properties compared to the arc-melted reference samples. Genarally, arc-melted processing has a higher vacuum level than induction-melted processing which is benificial to reduce the impurities. Also the remelting for several time can help to reduce the contaminations. The obtained samples showed different structures and mechanical properties. With SEM micrographs, it could be seen that the surface structure of arc-melted $Al_{0.5}CrFeCoNiCu$ samples were dendrite-like and alligned in all orientations. By contrast, the induction-melted samples were dendrite-like and had larger grain sizes. Also a sulfur contamination was found in $Al_{0.5}CrFeCoNiCu$ samples by EDS map. However, the distribution of metallic phases was similar. Chromium, cobalt and iron phases were mainly located in dendrite regions while copper phases gathered in interdendrite regions.

With X-ray diffraction, arc-melted samples showed fcc-structured while induction-melted samples showed dual-phase structures which contained fcc and bcc structures. By combining the structures and mechanical properties of these two samples, hard and brittle materials found in induction-melted samples. On the contrary, arc-melted samples behaved ductile.

The addition of molybdenum also had an imapct on the structures and mechanical properties of HEAs. Even though $Al_{0.5}CrFeCoNiCu$ HEA and $Al_{0.5}CrFeCoNiCuMo_{0.25}$ HEA were casted in the same conditions, the crystalline structures were totally different. $Al_{0.5}CrFeCoNiCu$ HEA had a mixed structures and behaves brittle whereas $Al_{0.5}CrFeCoNiCuMo_{0.25}$ HEA had bcc and shows ductility. Molybdenum containing phase mainly occured in dendrite regions. Also dark spots consisted of molybdenum and sulfur contaminations were observed in SEM images. After compression test, the interdendrite regions deformed heavily since the copper phases were ductile and experienced a significant deformation during the compression test.

Induction-melted $Al_{0.5}CrFeCoNiCuMo_{0.25}$ HEA had lower yield strength compared to the reference one when compressed them in a high strain rate. And induction-melted $Al_{0.5}CrFeCoNiCu$ HEAs even showed extreme brittleness which meant the products were not suitable for industrial applications. It could be concluded that the induction-melted $Al_{0.5}CrFeCoNiCu$ samples showed poor mechanical properties and even some sulfur impurites occured. The sulfur impurities had a harmful influence on mechanical properties of HEAs since sulfur could react with other metallic elements and formed sulphides inclusions. In order to improve the cleanliness and refine the structures of HEAs, the ingot

should be remelted in a high vacuum level before casting. Although induction-melting is easy to control and can prevent alloying loss to some extend, it is better to melt the ingot by arc melting for several times during casting.

The cooling rate also influence the microstructures and properties of HEAs. Higher cooling rate induce severer sluggish diffusion effect which leads to smaller grain sizes by limiting the growing space of grains. Also the dendrite size is compressed with high cooling rate. High cooling rate also contributes to form simple phases instead of dual-phases. High hardness and yield strength can be obtained with high cooling rates.

For further study, it is also interesting to know how to get rid of sulfur impurities when casting HEAs after induction-melting. The possible methods are remelting the ingot for several times and improve the vacuum level during casting. Since the origin of sulfur contamination is unknown, it it recommaned to clean the furnace before using. Also, if simple structures and small grain sizes are desired, the high cooling rate is suitable for manufacturing processing. Thus, higher hardness and yield strength can be obtained. Besides, the thermal properties of HEAs can be studied in the future since the melting temperature and DTA curves obtained with different heating and cooling rate are also helpful factors when choosing the parameters of heat treatments of HEAs. Heat treatments is benificial to refine and alter the structures of HEA thus improve the mechanical properties.

6 REFERENCES

[1] Yang X, Zhang Y. Prediction of high-entropy stabilized solid solution in multi-component alloys. Mater Phys Chem 2012;132(2–3):233–8.
[2] Y.F. Ye, Q. Wang, J. Lu, High-entropy alloy: challenges and prospects, Materialstoday, July–August 2016, Pages 349–362
[3] Lin C, Tsai H, Bor H. Effect of aging treatment on microstructure and properties of high-entropy Cu0.5CoCrFeNi alloy. Intermetallics 2010;18:1244–50.
[4] Yeh JW, Chen SK, Lin SJ, Gan JY, Chin TS, Shun TT, et al. Nanostructured high-entropy alloys with multiple principal elements: novel alloy design concepts and outcomes. Adv Eng Mater 2004;6(5):299–303.
[5] Yeh JW. Recent progress in high-entropy alloys. Presentation at Changsha meeting; 2011.
[6] K.B. Zhang, Z.Y. Fu, J.Y. Zhang, J. Shi, W.M. Wang, H. Wang, Y.C. Wang, and Q.J. Zhang, J. Alloy. Compd. 502, 295, 2010.
[7] P.D. Jablonski and J.A. Hawk, Proceedings of the 2013 International Symposium on Liquid Metal Processing and Casting, ed. M.J.M. Krane, A. Jardy, R.L. Williamson and J.J. Beaman (Wiley, Hoboken, 2013), pp. 329–332.
[8] Chao Wang, Wei Ji, Zhengyi Fu. Mechanical alloying and spark plasma sintering of CoCrFeNiMnAl high-entropy alloy. Advanced Powder Technology 25 (2014).
[9] B.R. Braeckman, F. Boydens, H. Hidalgo, et al. High entropy alloy thin films deposited by magnetron sputtering of powder targets. Thin Solid Films 580 (2015) 71–76
[10] Akira T, Kenji A, Takeshi W, Kunio Y, Wei Zhang et al. High-Entropy Alloys with a Hexagonal Close-Packed Structure Designed by Equi-Atomic Alloy Strategy and Binary Phase Diagrams. Volume 66, 2014 , pp 1984-1992.
[11] Yeh JW, Lin SJ, Chin TS, Gan JY, Chen SK, Shun TT, et al. Formation of simple crystal structures in Cu–Co–Ni–Cr–Al–Fe–Ti–V alloys with multiprincipal metallic elements. Metall Mater Trans A 2004;35(8):2533–6.
[12] Ren B, Liu ZX, Li DM, Shi L, Cai B, Wang MX. Effect of elemental interaction on microstructure of CuCrFeNiMn high entropy alloy system. J Alloy Compd 2010;493:148–53.
[13] Guo S, Ng C, Lu J, Liu CT. Effect of valence electron concentration on stability of fcc or bcc phase in high entropy alloys. J Appl Phys 2011;109:103505.
[14] Li J, Yiping L, Wei W, Zhiqiang C, et al. Microstructure and Mechanical Properties of a $CoFeNi_2V_{0.5}Nb_{0.75}$ Eutectic High Entropy Alloy in As-cast and Heat-treated Conditions. No. 32, 2016, pp. 245-220.

[15] Chin-You H, Chien-Chang J, et al. Effect of Aluminum Content on Microstructure and Mechanical Properties of AlxCoCrFeMo0.5Ni High-Entropy Alloys. JOM, Vol. 65, No. 12, 2013.

[16] Andrew M, Christopher C.B, Mitchell L,S, et al. Plasma-Sprayed High Entropy Alloys: Microstructure and Properties of AlCoCrFeNi and MnCoCrFeNi. 2014.

[17] Wen-yi Huo, Hai-fang Shi, Xin Ren, and Jing-yuan Zhang. Microstructure and Wear Behavior of CoCrFeMnNbNi High-Entropy Alloy Coating by TIG Cladding. Advances in Materials Science and Engineering. Volume 2015 (2015), Article ID 64735.

[18] Sicong Fang, Weiping Chen, Zhiqiang Fu. Microstructure and mechanical properties of twinned $Al_{0.5}CrFeNiCo_{0.3}C_{0.2}$ high entropy alloy processed by mechanical alloying and spark plasma sintering Materials and Design 54 (2014) 973–979.

[19] Li Jiang, Yiping Lu, Yong Dong, et al. Annealing effects on the microstructure and properties of bulk high-entropy $CoCrFeNiTi_{0.5}$ alloy casting ingot Intermetallics 44 (2014) 37e43.

[20] S. Liu, M.C. Gao, P.K. Liaw, et al. Microstructures and mechanical properties of $Al_xCrFeNiTi_{0.25}$ alloys. Journal of Alloys and Compounds 619 (2015) 610–615.

[21] Tsai CW, Tsai MH, Yeh JW, Yang CC. Effect of temperature on mechanical properties of Al0.5CoCrCuFeNi wrought alloy. J Alloy Compd 2010;490(1–2):160–5.

[22] Hemphill MA, Yuan T, Wang GY, Yeh JW, Tsai CW, Chuang A, et al. Fatigue behavior of Al0.5CoCrCuFeNi high-entropy alloys. Acta Mater 2012;60(16):5723–34.

[23] Ma SG, Zhang Y, Liaw PK. Damping behaviors of AlxCoCrFeNi high-entropy alloys by a dynamic mechanical analyzer, J Alloy Compd, in preparation.

[24] N. G. Jones, K. A. Christofidou and H. J. Stone. Rapid precipitation in an Al0.5CrFeCoNiCu high entropy alloy. 2015.

[25] Yeh JW. Recent progress in high-entropy alloys. Presentation at Changsha meeting; 2011.

[26] Yong Zhang, Tingting Zuo, et al. High-entropy Alloys with High Saturation Magnetization, Electrical Resistivity, and Malleability. Scientific Reports 3, Article number: 1455 (2013)

[27] B. Zhang, M.C.Gao, Y.Zhang, et al. Senary refractory high-entropy alloy CrxMoNbTaVW. ComputerCouplingofPhaseDiagramsandThermochemistry51(2015)193–201.

[28] The Vickers Hardness Testing Machine. Ukcalibrations.co.uk. Retrieved on 2016-06-03.

[29] Wei Ji, Zhengyi Fu, Weimin Wang, et al. Mechanical alloying synthesis and spark plasma sintering consolidation of CoCrFeNiAl high-entropy alloy. Journal of Alloys and Compounds 589 (2014) 61–66.

[30] Zhang Y, Yang X, Liaw PK. Alloy design and properties optimization of high-entropy alloys. JOM 2012;64(7):830–8.

[31] Yeh JW. Recent progress in high-entropy alloys. Ann Chim Sci Mater 2006;31(6):633–48.

[32] Yong Zhang, Ting Ting Zuo, Zhi Tang, Michael c. Gao, Krin A. Dahmen, et al. Progress in Materials Science. No.61, 2014, pp. 1-93.